

1 **Thermodynamic properties of the effector domains of MARTX toxins suggest**
2 **their unfolding for translocation across the host membrane**

3
4 Elena Kudryashova¹, David Heisler^{1,2}, Andrew Zywiec¹, Dmitri S. Kudryashov^{1,2,*}

5
6 ¹Department of Chemistry and Biochemistry, The Ohio State University, Columbus, OH, USA

7 ²The Ohio State Biochemistry Program, The Ohio State University, Columbus, OH, USA

8
9 *To whom correspondence should be addressed:

10 Dmitri S. Kudryashov
11 The Ohio State University
12 Department of Chemistry and Biochemistry
13 728 Bioscience Research Building
14 484 W 12th Ave
15 Columbus, OH, 43210, USA
16 Tel: (614) 292-4848
17 Fax: (614) 292-6773
18 E-mail: kudryashov.1@osu.edu

19
20
21
22 Running title: *Thermodynamic properties of MARTX effector domains*

23
24
25 Key words: *bacterial toxins, MARTX, molten globule, thermal and chemical*
26 *denaturation, membrane translocation*

This article has been accepted for publication and undergone full peer review but has not been through the copyediting, typesetting, pagination and proofreading process, which may lead to differences between this version and the Version of Record. Please cite this article as doi: 10.1111/mmi.12615

This article is protected by copyright. All rights reserved.

27

28 **SUMMARY**

29 MARTX (multifunctional autoprocessing repeats-in-toxin) family toxins are produced by
30 *V.cholerae*, *V.vulnificus*, *A.hydrophila* and other Gram-negative bacteria. Effector domains of
31 MARTX toxins cross the cytoplasmic membrane of a host cell through a putative pore formed
32 by the toxin's glycine-rich repeats. The structure of the pore is unknown and the translocation
33 mechanism of the effector domains is poorly understood. We examined the thermodynamic
34 stability of the effector domains of *V.cholerae* and *A.hydrophila* MARTX toxins to elucidate the
35 mechanism of their translocation. We found that all but one domain in each toxin are
36 thermodynamically unstable and several acquire a molten globule state near human
37 physiological temperatures. Fusion of the most stable cysteine protease domain to the
38 adjacent effector domain reduces its thermodynamic stability ~1.4 fold (from $\Delta G^{\text{H}_2\text{O}}$ 21.8 to
39 16.1 kJ/mol). Precipitation of several individual domains due to thermal denaturation is
40 reduced upon their fusion into multi-domain constructs. We speculate that low thermostability
41 of the MARTX effector domains correlates with that of many other membrane-penetrating
42 toxins and implies their unfolding for cell entry. This study extends the list of thermolabile
43 bacterial toxins, suggesting that this quality is essential and could be susceptible for selective
44 targeting of pathogenic toxins.

45

46 INTRODUCTION

47 Multifunctional autoprocessing repeats-in-toxin (MARTX) toxins are produced by several
48 Gram-negative bacteria among which are *Vibrio cholerae*, *Vibrio vulnificus*, *Vibrio*
49 *anguillarum*, *Vibrio splendidus*, *Yersinia enterocolitica*, *Aeromonas hydrophila*, and other
50 pathogens of human, animal, and marine life infectious diseases. MARTX toxins belong to a
51 superfamily of RTX (repeats-in-toxin) toxins, yet they differ substantially from other members
52 of the family in several important aspects. MARTX toxins, with their 350-550 kDa size, are
53 not only substantially larger than other RTX toxins, but are also the largest single polypeptide
54 chain toxins discovered to date (Fig. 1A). Next, the Ca²⁺-binding GD-rich 9-aa repeats
55 (consensus motif G-xx-G-x-N/D), which the entire RTX family was named after, are
56 substituted in MARTX toxins with closely related 18-aa repeats (called C-repeats) with a
57 predicted ability to bind one Ca²⁺ ion per repeat (Satchell, 2011). Additionally, MARTX toxins
58 have two other unique glycine-rich types of repeats named type A and type B (Satchell,
59 2007). All of these repeats share a common G-7x-G-xx-N motif and are therefore likely to
60 have structural similarity. In a typical MARTX toxin, 14 copies of 20-aa A repeats are located
61 at the N-terminus, followed by 38 copies of 19-aa B repeats, whereas the GD-rich RTX-like
62 C-repeats are located at the C-terminus (Fig. 1A) (Satchell, 2011). The number and the
63 sequences of all three repeats are well conserved in the majority of MARTX toxins with only
64 few minor exceptions (Satchell, 2007). These repeats have been proposed to cooperate for
65 delivery of several (1 to 5) effector domains followed by a conserved cysteine protease
66 domain (CPD) (Satchell, 2011).

67 By analogy with pore-forming RTX toxins (Lally *et al.*, 1999), it has been proposed that
68 the repeat domains of MARTX form a pore-like structure utilized for translocation of the
69 MARTX effector domains into the cytoplasm of a host cell (Satchell, 2007). The pathogenic
70 effects of MARTX toxins stem mainly from the specific activities of the respective effector
71 domains. Composition of the effector domains varies between MARTX toxins of different
72 species as well as different biotypes of a same species due to genetic recombination with
73 other MARTX toxins encoded either genomically or in mobile elements (Kwak *et al.*, 2011,
74 Roig *et al.*, 2011). CPD is the only invariable internal domain shared by all MARTX toxins.
75 CPD is a cysteine protease that is activated only upon crossing the cytoplasmic membrane
76 via interaction with cytoplasmic inositol hexakisphosphate (InsP₆); once activated, CPD
77 cleaves off other effector domains and releases them from the membrane-bound repeats

78 (Prochazkova & Satchell, 2008, Prochazkova *et al.*, 2009, Shen *et al.*, 2009, Egerer &
79 Satchell, 2010).

80 Apart from CPD, other effector domains of *V. cholerae* MARTX toxin (MARTX_{Vc}) include:
81 actin crosslinking domain (ACD), Rho GTPase inactivation domain (RID), and a domain with
82 a characteristic α/β -hydrolase fold (ABH). The *A. hydrophila* MARTX toxin (MARTX_{Ah}) also
83 has ACD and ABH domains, but no RID. Other MARTX_{Ah} domains absent in MARTX_{Vc}
84 include PMT (similar to the C-terminal region of *Pasteurella multocida* toxin) and MCF
85 (similar to “makes caterpillars floppy” toxin) (Fig 1). Both RID and ACD target the actin
86 cytoskeleton. RID indirectly inhibits Rho family GTP-ases by an unknown mechanism
87 (Sheahan & Satchell, 2007, Pei & Grishin, 2009, Ahrens *et al.*, 2013), whereas ACD
88 covalently crosslinks monomeric actin via an isopeptide bond (Kudryashov *et al.*, 2008a,
89 Kudryashova *et al.*, 2012) resulting in the accumulation of actin oligomers incapable of
90 polymerization (Kudryashov *et al.*, 2008b). Therefore, both domains induce disassembly of
91 the actin cytoskeleton in affected cells (Cordero *et al.*, 2006, Sheahan & Satchell, 2007) and
92 a subsequent neutralization of the immune potential of macrophages and neutrophils (Queen
93 & Satchell, 2012). The functional roles of other effector domains are currently unknown.

94 Effector domain translocation is not affected by inhibition of endocytosis (Sheahan *et al.*,
95 2004) and therefore is likely to occur directly across the host cytoplasmic membrane and not
96 through the endosomal pathway. However, neither the host cell receptor elements targeted
97 by MARTX toxins are currently recognized, nor are the mechanisms of effector domain
98 delivery to the cytoplasm known. In the absence of direct experimental evidence, analogy
99 with pore-forming RTX toxins has been made to postulate that the repeat domains of MARTX
100 form a pore-like structure in the host cytoplasmic membrane used as a tunnel for
101 translocation of the effector domains directly to the host cell cytoplasm (Satchell, 2007). The
102 size and permeability of the tentative pore for substances other than effector domains is a
103 subject of controversy. Thus, no open pore was reported for *V. cholerae* MARTX toxin
104 (Fullner & Mekalanos, 2000); whereas formation of an open pore with a diameter of ~1.6 nm
105 was suggested for *V. vulnificus* MARTX toxin based on 50% inhibition of hemolytic activity of
106 the toxin by polyethylene glycol molecules of this size (Kim *et al.*, 2008). It has been
107 proposed that along with the effector domain composition, the size of the formed pore may
108 account for difference in toxicity between MARTX toxins (Kim *et al.*, 2008).

109 As the mechanism of translocation is unknown, it is not clear whether the effector
110 domains are transported unfolded or in their folded state, and what is the thermodynamic

111 gradient fueling this translocation. Membrane structures of MARTX toxins have never been
112 observed, and direct investigation of the molecular mechanisms of the effector domain
113 delivery across the host membrane is hindered by limited availability of full-length MARTX
114 toxins. Indeed, the toxins are difficult to express ectopically due to their enormous size (~0.5
115 MDa) and are problematic to purify in substantial amounts from toxin-producing
116 microorganisms due to small quantities produced, and sophisticated regulation of expression
117 initiated only upon direct contact with the host cells and ceased soon after (Kim *et al.*, 2008,
118 Lee *et al.*, 2008). We postulate that a mechanism of effector domains' delivery is encoded in
119 and, therefore, can be deduced from their structural/thermodynamic properties, even though
120 the structure of the transportation machinery *per se* (e.g. MARTX transmembrane repeats) is
121 not known. A high degree of thermodynamic instability often indicates that the domains are
122 transported in partially or completely unfolded states (e.g. LF and EF of anthrax toxin (Krantz
123 *et al.*, 2004, Krantz *et al.*, 2006, Thoren *et al.*, 2009, Feld *et al.*, 2010, Wynia-Smith *et al.*,
124 2012), *Clostridium difficile* TcdA and TcdB toxins (Salnikova *et al.*, 2008)). On the other hand,
125 thermodynamically stable proteins or protein-ligand complexes would likely get transported in
126 their fully folded states (e.g. by the twin arginine translocation (TAT) pathway across bacterial
127 membranes (Lee *et al.*, 2006)). Therefore, considering the aforementioned limitations, we
128 focused on probing thermodynamic properties of MARTX effector domains from *V. cholerae*,
129 a mesophilic pathogen (Miller *et al.*, 1984), and *A. hydrophila*, a psychrotrophic bacterium
130 that can thrive under moderately cold (5-15°C) conditions (Grau, 1981), in order to recognize
131 their common characteristics. We reasoned that using two toxins from organisms optimized
132 for growth at different temperature conditions should provide a broader context for testing the
133 proposed hypothesis.

134 We found that all effector domains of MARTX are notably unstable compared to typical
135 mesophilic proteins and several effector domains, particularly the peripheral ones, melt via
136 molten globule intermediates. Furthermore, fusion of two or more individual domains into a
137 single polypeptide chain decreases precipitation upon thermal unfolding/denaturation of the
138 effector domains, increases the cooperativity of melting, strictly reduces variability in the
139 transition points, and decreases the melting temperature and thermal stability to a value
140 demonstrated by the least stable domains. Intriguingly, although CPD domain is relatively
141 stable on its own, it is destabilized upon fusion to adjacent domains. Thus, free energy
142 change of CPD_{vc} unfolding decreases ~1.4 fold upon its fusion to the adjacent ABH_{vc}
143 domain. Therefore, our data support the hypothesis that low thermodynamic stability of the
144 MARTX effector domains bestows their unhindered unfolding near host physiological

145 temperatures needed for the efficient translocation across the host membrane. Notably,
146 thermodynamic instability demonstrated by the effector domains of MARTX toxins is shared
147 with at least several other membrane-penetrating toxins (LF and EF of *Bacillus anthracis*
148 (Krantz *et al.*, 2004, Krantz *et al.*, 2006), TcdA and TcdB of *Clostridium difficile* (Salnikova *et*
149 *al.*, 2008), Listeriolysin O of *Listeria monocytogenes* (Schuerch *et al.*, 2005), and CTA1
150 subunit of cholerae toxin (Pande *et al.*, 2007)), but not by extracellular host proteins. We
151 speculate that this property is essential for a wide range of membrane-penetrating/pore-
152 forming toxins and can be targeted for toxin inactivation.

153

154 RESULTS

155 **Activity of the ACD effector domains of MARTX reaches maximum at sub-**
156 **physiological temperatures.** To test the hypothesis that a common mechanism of
157 translocation of MARTX effector domains across the host membrane calls for similarities in
158 their thermodynamic properties, we chose to examine two MARTX toxins produced by Gram-
159 negative bacteria adapted to different temperature environments - mesophilic *V. cholerae*
160 (MARTX_{Vc}) and psychrotrophic *A. hydrophila* (MARTX_{Ah}). To streamline identification of the
161 properties in common among these effector domains, we first selected to focus on one of the
162 most functionally and structurally characterized ACD domains present in both MARTX toxins
163 as a model protein for detailed analysis. The ACD_{Vc} functional enzymatic activity is well
164 portrayed (Kudryashova *et al.*, 2012, Kudryashov *et al.*, 2008b, Kudryashov *et al.*, 2008a,
165 Cordero *et al.*, 2006); and the crystal structure of the closely related ACD domain of VgrG1
166 toxin of *V. cholerae* has been recently solved (Durand *et al.*, 2012).

167 Upon delivery to the cytoplasm of the host immune cell, ACD works as an actin-specific
168 protein ligase that phosphorylates the E270 residue on one actin molecule (Kudryashova *et*
169 *al.*, 2012) and then crosslinks it to K50 on another actin molecule via an amide (isopeptide)
170 bond (Kudryashov *et al.*, 2008b, Kudryashova *et al.*, 2012). This crosslinking leads to
171 formation of polymerization-incompetent actin oligomers and disrupts the cytoskeleton
172 (Cordero *et al.*, 2006, Kudryashov *et al.*, 2008a, Kudryashov *et al.*, 2008b). We determined
173 the rates of enzymatic activity of ACD_{Vc} and ACD_{Ah} *in vitro* at different temperatures by
174 following the accumulation of crosslinked actin species during the linear stage of the reaction
175 (Fig. 2A). We found that the rate of activity has a characteristic bell-shaped temperature
176 dependence profile with the optimal activity between 31 - 34°C for ACD_{Vc} and 22 - 25°C for
177 ACD_{Ah} (Fig. 2B). Remarkably, ACD_{Ah} retains at least 50% of its activity in the broad range

178 from 5 to 34°C, which likely reflects the adaptation of *A. hydrophila* to life in both cold and
179 warm waters. Typically, an enzyme activity peaks at or slightly above the environmental
180 temperature (Somero, 1995) and, therefore, the ACD_{Vc} activity seems to be optimized not to
181 the human body, but to other hosts. Alternatively, higher than expected thermal sensitivity of
182 ACD_{Vc} may reflect that its structural flexibility was acquired for a reason other than thermal
183 adaptation. To test this hypothesis, we analyzed chemical and thermal denaturation of ACD
184 and other effector domains of MARTX toxins from *V. cholerae* and *A. hydrophila*.

185 **Chemically induced denaturation of ACD_{Vc}.** Eight tryptophan residues of ACD_{Vc} are
186 evenly spaced throughout the sequence and therefore can serve as reliable reporters of
187 protein denaturation. To determine free energy change (ΔG_o) of the ACD_{Vc} unfolding, we
188 monitored intrinsic Trp fluorescence of ACD_{Vc} in the presence of increasing concentrations of
189 guanidinium hydrochloride (GdnHCl) and urea (Fig. 3). Exposure of Trp residues to solvents
190 due to denaturant-induced unfolding of a protein results in a red shift of the wavelength
191 maximum (λ_{max}) of Trp emission spectra (Fig. S1A,B). In both denaturants, a prompt shift of
192 λ_{max} was detected that reached the maximum at 1.5 M GdnHCl and 3 M urea, reflecting
193 exposure of Trps to solvent due to the protein unfolding (Fig. 3). The Trp λ_{max} transition
194 curves fit well to a single-step sigmoidal equation (equation 5 with sloping baselines in
195 Experimental Procedures) with transition midpoints at 0.87 M and 1.67 M for GdnHCl and
196 urea, respectively. Assuming a two-state transition model, free energy changes of ACD_{Vc}
197 unfolding for a given denaturant concentrations (ΔG) were calculated (Fig. 3A,B – inserts)
198 and free energy differences of unfolding in the absence of denaturant (ΔG^{H_2O}) converged well
199 to 11.5 kJ/mol and 11.4 kJ/mol for GdnHCl- and urea-induced denaturation, respectively.
200 Given that ΔG^o for most proteins is in the 20-65 kJ/mol range (Park & Marqusee, 2004), it
201 can be concluded that ACD_{Vc} is substantially (~ 2 - 6 fold) less stable than an average
202 mesophilic protein and similar in this sense to proteins produced by psychrophilic (adapted to
203 cold) organisms (Feller, 2010, Feller & Gerday, 2003).

204 **Thermal unfolding of tertiary and secondary structures of ACD_{Vc}.** To discriminate
205 between unfolding of secondary and tertiary structures of ACD_{Vc}, a combination of far- and
206 near-UV circular dichroism (CD) spectroscopy was employed. Whereas far-UV CD signals
207 report changes in secondary structure elements (α -helices, β -sheets, loops), the near-UV CD
208 signals detect changes in aromatic residues and disulfide bonds and can reveal perturbations
209 of tertiary structure in proximity to these elements (Kelly & Price, 2000).

210 At sub-transition temperatures, the far-UV spectrum of ACD_{Vc} showed two characteristic

211 minima at 208 nm and 222 nm typical for helical proteins (Fig. 4A; S2A). The α -helical
212 content calculated from our experimental CD data using K2D3 software program (Louis-
213 Jeune *et al.*, 2011) correlates well with the X-ray data obtained from a homologous X-ray
214 structure of *V. cholerae* VgrG1 ACD (pdb: 4DTH) (Durand *et al.*, 2012) (31.13% versus 31%,
215 respectively); whereas β -sheet content differs from the X-ray data by 5.6% (15.44% versus
216 21% determined from the crystal structure). The small discrepancy in the latter case may
217 reflect a difference between the homologous ACD domains of MARTX_{Vc} and VgrG1_{Vc} or stem
218 from differences in experimental techniques and/or conditions.

219 Monitoring the ACD_{Vc} thermal unfolding via far-UV CD at 208 nm revealed relatively
220 minor non-cooperative changes of low amplitude between 30 and 50°C, at which point a
221 steep transition occurred with an apparent half-transition point at 53.6°C (Fig. 4B). Recording
222 the entire far-UV spectra at various temperatures confirmed that the major changes in the
223 ACD_{Vc} secondary structure happened at >52°C with only minor changes detected at lower
224 temperatures (Fig. 4A). Simultaneous rise in dynode voltage showed that the steep
225 secondary structure transition coincided with protein precipitation (Fig. 4B – black line)
226 (Benjwal *et al.*, 2006).

227 The near-UV CD spectrum of ACD_{Vc} is characterized by two prominent dips at 283 and
228 290 nm related to signals from Tyr and Trp residues (Fig. 4C, S2B). Both dips were greatly
229 diminished upon transition from 34 to 42°C, and completely leveled at 46°C, before the entire
230 spectra collapsed at 48°C (Fig. 4C) due to the protein aggregation (as evidenced from the
231 simultaneous increase of dynode voltage; Fig. 4D - black line). Even though the 290 nm dip
232 was mostly or completely leveled before the aggregation occurred, only the onset
233 temperature of tertiary structure unfolding (~34°C) and not the half-transition point was
234 extracted from this experiment to avoid over interpretation. Therefore, in the range of 30 -
235 45°C (before the occurrence of precipitation) the perturbations in the tertiary structure of
236 ACD_{Vc} were substantial, whereas the secondary structure remained mainly preserved. This
237 suggests that under physiological temperature of human body (~37°C) ACD_{Vc} partially exists
238 in a molten globule state, i.e. with a tertiary structure less defined than that in the fully folded
239 protein, but more compact than in a random coil state (Ohgushi & Wada, 1983). Interestingly,
240 the difference between thermal transitions in far- and near-UV is preserved in the
241 homologous *A. hydrophila* ACD_{Ah} protein even though both far- and near-UV melting profiles
242 of this protein were shifted to 10-15°C lower temperatures (Fig. S3A,B; S4A,B), likely
243 reflecting the adaptation of this pathogen to cold conditions.

244 Noteworthy, our Trp fluorescence chemical denaturation data imply a two-state (native
245 and denatured) transition for ACD_{vc} unfolding, while unfolding through a molten globule
246 intermediate imposed by the CD results suggests three states (native, molten globule, and
247 denatured). Applying the three-state model to fit the Trp data generated nearly identical
248 curves, albeit with much greater errors for the fit parameters (Fig. S1C,D). A possible
249 explanation for this discrepancy is that Trp fluorescence characteristics of two of the ACD_{vc}
250 transition states (native and molten globule, or molten globule and unfolded states) are not
251 sufficiently different and therefore evade detection.

252 **Effector domains of MARTX toxins from two different microorganisms are**
253 **thermolabile.** If low thermodynamic stability indeed plays an important role in transport of
254 ACD across the host membrane, then other MARTX effector domains should also have
255 similar thermodynamic properties. To test this hypothesis, we examined individual effector
256 domains of MARTX toxins from *V. cholerae* and *A. hydrophila* using far- and near-UV CD
257 spectroscopy (Fig. 5A,B; S2-4; Table 1).

258 Interestingly, all six analyzed effector domains of MARTX toxins showed onsets of
259 thermal denaturation at or below 35°C either in the near-, far-, or both UV regions; i.e.
260 demonstrated thermal instability. CD data did not allow for confident detection of a molten
261 globule state for MARTX effector domains other than ACD. We reasoned that this might
262 reflect a context dependence and insufficient sensitivity of near-UV CD for revealing tertiary
263 structure perturbations due to their dependence on particular positioning of Trp, Tyr, and
264 disulfide bonds in a protein. To overcome this drawback, we employed differential scanning
265 fluorimetry (DSF) as an alternative method for monitoring protein unfolding.

266 DSF is based on a rise of fluorescence of an environmentally sensitive dye (e.g. 8-
267 anilinonaphthalene-1-sulfonic acid (ANS) or, in our case, SYPRO Orange) upon interaction
268 with a denaturation-exposed hydrophobic interior of a protein (Niesen *et al.*, 2007). DSF
269 showed that most (five out of six) of the individual effector domains of both MARTX toxins
270 melt at temperatures close to that of the human body ($T_m \approx 34-44$ °C) (Fig. 6A,B; Table 1);
271 whereas the sixth domain (ACD_{Ah}) undergoes transition at a substantially lower temperature
272 of ~27°C. Notably, for four domains (all the effector domains of MARTX_{vc} and ACD_{Ah}) the
273 phase transition temperatures detected by DSF were 8-14°C lower compared to those
274 measured by far-UV CD with the largest difference observed for both ACD_{Ah} and ACD_{vc}
275 domains (13 and 14°C, respectively). The observed differences suggest that DSF reports

276 tertiary structure changes that precede the unfolding of secondary structure elements
277 detected by far-UV CD.

278 Importantly, far-UV CD spectra of ACD_{Vc} and both CPD domains acquired in the
279 presence of SYPRO Orange showed that there is only marginal (0 - 2°C) destabilizing effect
280 of the dye on the unfolding of their secondary structure (Fig. S5), which cannot be held
281 responsible for the observed differences between the melting temperatures detected by DSF
282 and CD approaches. Although we cannot rule out that SYPRO Orange can destabilize native
283 conformation of a protein by binding and stabilizing a partially unfolded state, our data implies
284 that the concentration of the dye used in the study is not sufficient to cause strong
285 destabilization effect. This assumption is supported by our finding that DSF melting points for
286 MPT_{Ah}, ABH_{Ah}, and PMT-CPD_{Ah} were nearly identical to those detected by far-UV CD in the
287 absence of the dye. It is also possible that different effector domains vary in their sensitivity to
288 the destabilizing effects of the dye, which can therefore magnify the difference between the
289 native to molten globule and molten globule to unfolded state transitions.

290 Therefore, at the human body physiological temperature all effector domains of
291 MARTX_{Vc} and at least one domain of MARTX_{Ah} (ACD_{Ah}) exist in equilibrium between fully
292 folded and partially unfolded molten globule states. The observed low thermodynamic
293 stability of individual domains agrees with a hypothesis that at least partial unfolding of the
294 effector domains is required for their translocation across the host membrane (Satchell, 2007,
295 Egerer & Satchell, 2010).

296 **Thermostability of CPD domains.** Formally speaking, MARTX CPD is not an effector
297 domain as it does not directly exert toxicity to host cells. Yet, its delivery to the cytoplasm of
298 host cells should obey the same constraints. Interestingly, CPD of both *V. cholerae* and *A.*
299 *hydrophila* demonstrate substantially higher thermal stability ($T_m = 54/48^\circ\text{C}$ and $60/51^\circ\text{C}$, as
300 detected by far-UV CD/DSF, respectively) (Table 1). We verified that this stability is not due
301 to the buffer compositions used in our CD or DSF experiments, since neither sodium
302 phosphate (50 mM) nor sodium chloride (150 mM) had any effect on DSF T_m of CPD and
303 only marginally (1°C difference) affected its CD T_m (Fig. S6). Therefore, such high stability of
304 CPD implies that either unfolding is not required for its translocation, or that some
305 unaccounted factors adversely affect the stability of the CPD domains upon their cytoplasmic
306 delivery. Indeed, it has been reported earlier that CPD of *V. cholerae* is thermodynamically
307 unstable and undergoes thermal denaturation at about 38°C (detected by DSF) unless
308 stabilized by inositol hexakisphosphate (InsP₆) – a cytoplasmic activator of the CPD protease

309 activity (Prochazkova *et al.*, 2009). However, a “post-cleavage” conformation of the enzyme
310 has been found to be substantially more stable than a “pre-cleavage” (and subsequently a
311 “pre-transition”) state (Prochazkova *et al.*, 2009). CPD constructs used in our study do not
312 contain the key Leu residue in the self-cleavage substrate recognition site at the N-terminus
313 of the protease domains. Identical DSF melting points (47°C) of our CPD construct and the
314 processed post-CPD (Prochazkova *et al.*, 2009) under identical buffer conditions, strongly
315 suggest that they both represent the “post-cleavage” CPD state even though prepared in
316 entirely different ways.

317 If the above supposition is correct, CPD should adopt a more pliable “pre-cleavage”
318 conformation in conjunction with MARTX effector domains (substrates of CPD) and in the
319 absence of InsP₆, and CPD’s unfolding should proceed with a similar minimal investment of
320 energy as the unfolding of other domains. Indeed, in agreement with this assumption the
321 tertiary and secondary structures of most larger CPD-containing constructs undergo thermal
322 denaturation at 36 - 38°C and 42 - 44°C, respectively; whereas the five-domain *A. hydrophila*
323 construct melts at even lower temperatures of 28°C and 37°C (Fig. 5C,D; 6C,D; Table 1).

324 ***Mutual effects of adjacent domains on their stability.*** Since all MARTX effector
325 domains are transported across the host membrane together as a single polypeptide chain,
326 we tested whether the domains exhibit mutual influence (stabilization or destabilization) when
327 expressed as fusion proteins (Fig. 1B-D; S7; S8). First, we found that fusion of two or more
328 individual domains into a single polypeptide chain decreased or abolished precipitation upon
329 thermal unfolding/denaturation, so that RID-ABH_{VC} and ACD-RID-ABH-CPD_{VC} constructs
330 showed no signs of precipitation (Table 1, Fig. S9). Next, CD and DSF both showed that
331 none of the tested constructs were more stable than their individual components (Fig. 5; 6;
332 S7-9; Table 1). On the contrary, most of the tested fusion domains of both MARTX toxins
333 underwent thermal transitions near the melting temperatures of the least stable domains,
334 whereas in some cases (ACD-ABH_{Ah}) the domains appeared to be mutually destabilized (i.e.
335 melted at the temperature slightly lower than that of the least stable element). Tertiary
336 structure of all fusion domains of MARTX_{VC} was melted at a nearly identical temperature of
337 37°C; whereas unfolding of secondary structure elements detected by far-UV CD occurred at
338 43-44°C with the single exception of ACD-RID_{VC}, for which secondary elements melted at
339 ~48°C (Fig. 5; Table 1). Next, melting profiles of the fused ACD-containing effector domains
340 of MARTX_{Ah} were less stable ($T_m \approx 25-30^\circ\text{C}$) than other constructs.

341 We recognize that the accurate detection of individual transitions in multidomain protein
342 toxins can be hindered by a higher affinity of SYPRO Orange to the least stable domain (in
343 DSF) or by protein precipitation (both in DSF and CD) and therefore can lead to
344 misinterpretation of the melting profiles. However, we contend that aggregation cannot be
345 held accountable, at least for the observed low stability of the CPD_{VC}-containing constructs
346 (ABH-CPD_{VC} and ACD-RID-ABH-CPD_{VC}; Fig. S9E,I; Table 1), since these constructs undergo
347 thermal unfolding without detectable precipitation.

348 To further verify that the observed destabilization is not due to the limitations of the
349 experimental techniques discussed above, we compared $\Delta G^{\text{H}_2\text{O}}$ of CPD_{VC} alone with that of
350 the same domain in a fusion construct ABH-CPD_{VC} using CPD-specific spectroscopic probes.
351 First, we took advantage of the intrinsic fluorescence of three tryptophans present in CPD_{VC},
352 whereas ABH_{VC} is naturally void of Trp residues. In agreement with our DSF/CD results, we
353 found that CPD_{VC} alone ($\Delta G^{\text{H}_2\text{O}}=21.8$ kJ/mol) is 1.4 times more stable than in the fusion form
354 with ABH_{VC} (16.1 kJ/mol) (Fig. 7A). These results confirmed that indeed, CPD_{VC} is
355 destabilized by the adjacent ABH_{VC} domain. Next, we selectively modified CPD_{VC} by two
356 different thiol-specific reagents in attempt to benefit from a single Cys residue present in
357 CPD_{VC}, but not in ABH_{VC}. However, introduction of either pyrene or acrylodan to label Cys
358 residue strongly destabilized CPD as revealed by $\Delta G^{\text{H}_2\text{O}}$ differences calculated from changes
359 in Trp or acrylodan/pyrene fluorescence upon urea denaturation (Fig. 7B; S10). Based on this
360 similarity, we speculate that a substrate-mediated destabilization of CPD (as well as its
361 elevated affinity to InsP₆ (Prochazkova & Satchell, 2008)) may also be triggered by direct
362 interaction of a substrate with the catalytic cysteine.

363 Furthermore, in agreement with our far-UV CD and DSF data, we found that fusion of
364 ABH_{VC} (which has no Trp residues) to RID_{VC} (has 10 Trp residues) results in mild but
365 statistically significant destabilization of RID_{VC} ($\Delta G^{\text{H}_2\text{O}}=11.5$ kJ/mol, compared to $\Delta G^{\text{H}_2\text{O}}$ of
366 RID_{VC} alone 13.2 kJ/mol; Fig. S11).

367 It can be noted that while fusion of ABH_{VC} to RID_{VC} reduces its stability to the identical
368 value calculated for ACD_{VC} (11.5 kJ/mol), the $\Delta G^{\text{H}_2\text{O}}$ values for ABH-CPD_{VC} and ACD_{VC} still
369 vary by 4.6 kJ/mol (16.1 versus 11.5 kJ/mol, respectively) and therefore they might still melt
370 as separate domains in the 4-domain fusion construct, but with melting characteristics very
371 similar to each other. Alternatively, the CPD domain can be further destabilized by other N-
372 terminal domains (e.g. ACD) by unexplored mechanisms.

373

374 DISCUSSION

375 In the current work we analyzed thermodynamic properties of the effector domains of *V.*
376 *cholerae* and *A. hydrophila* MARTX toxins and found that they have low thermostability. It
377 can be recognized that the low thermodynamic stability of MARTX effector domains correlate
378 with that of many membrane-penetrating toxins studied earlier and therefore likely become
379 evolved to facilitate their transition through the host membrane in a partially or fully unfolded
380 state.

381 The majority of tested individual MARTX effector domains melt via a molten globule
382 intermediate as demonstrated by a significant (up to 14°C) difference between unfolding of
383 tertiary and secondary structures detected by DSF and far-UV CD, respectively (Table 1). It
384 has been theoretically predicted that due to its conformational plasticity and ability to
385 accommodate to both polar and nonpolar environments, molten globules can be crucial for
386 protein transport across a membrane (Bychkova *et al.*, 1998). Indeed, molten globule states
387 have been demonstrated for several bacterial toxins, including LF and EF subunits of anthrax
388 toxin (Krantz *et al.*, 2004, Krantz *et al.*, 2006), *Escherichia coli* colicin A (van der Goot *et al.*,
389 1991, Lakey *et al.*, 1992), diphtheria toxin (Zhao & London, 1986, Ren *et al.*, 1999),
390 botulinum neurotoxin A (Cai *et al.*, 2006, Hasani *et al.*, 2009), and *E. coli* α -hemolysin (Herlax
391 & Bakas, 2007). Remarkably, similar to the effector domains of MARTX toxins, many of
392 these, as well as other bacterial toxins, are known to unfold at or near the human
393 physiological range of temperatures. The list of other thermolabile toxins includes
394 Listeriolysin O of *L. monocytogenes* ($T_m \approx 37^\circ\text{C}$; (Schuerch *et al.*, 2005)), TcdB ($T_m \approx 40^\circ\text{C}$) and
395 TcdA ($T_m \approx 45^\circ\text{C}$) toxins of *C. difficile* (Salnikova *et al.*, 2008), CTA1 subunit of cholera toxin
396 ($T_m \approx 37^\circ\text{C}$; (Pande *et al.*, 2007)), and lethal factor (LF) of *B. anthracis* ($T_m \approx 42^\circ\text{C}$ with an onset
397 of unfolding at 30°C ; (Gupta *et al.*, 2001)).

398 Thermodynamically, a fully unfolded protein appears to be an even better substrate for
399 translocation through a narrow pore than molten globules. However, we rationalize that
400 compared to the fully unfolded proteins, molten globules have better chances to withstand
401 aggregation and harsh environmental conditions (such as those created by proteases and
402 defense peptide attacks orchestrated by the host immune system). We speculate that there
403 are evolutionary advantages for bacterial toxins to adopt molten globule rather than the
404 unfolded state and, therefore, molten globules play an important role in the pathophysiology
405 of bacterial toxins. Hence, it is reasonable to propose that the tendency of MARTX domains
406 to form a molten globule at near physiological temperatures is an essential part of the

407 translocation mechanism. Conversely, it appears that the formation of a molten globule is not
408 a common property of all MARTX effector domains and, therefore, the domains, which unfold
409 through a molten globule state, may play a priming role in other domains' unfolding required
410 for translocation. Thus, ACD domains of both MARTX toxins form very prominent molten
411 globules ($\Delta T_m=13 - 14^\circ\text{C}$; Table 1). It is noteworthy that whenever present in MARTX toxins,
412 ACD is always the most N-terminally located effector domain (Satchell, 2011) and tentatively
413 might play an important role in unfolding of the entire structure and/or formation of a molten
414 globule, thus aiding in the translocation process.

415 ACD domains of both toxins share characteristic shapes of far- and near-UV CD spectra
416 (Fig. S2A,B and S3A,B), well defined molten globule states, nearly identical differences
417 between tertiary and secondary structure melting temperatures (13 and 14°C ; Table 1), and
418 overall shapes of phase transition profiles (Fig. S4A and B). Remarkably, despite a high
419 sequence similarity between the two ACD domains (80%), ACD of *A. hydrophila* has lower
420 optimal activity temperature (22 - 25°C versus 31 - 34°C) and is even less stable than its *V.*
421 *cholerae* counterpart as its tertiary and secondary structures melt at 12 - 13°C lower
422 temperatures (27.4 versus 39.7°C and 40.2 versus 53.6°C , respectively). Although not
423 psychrophilic (as it has an optimum of growth temperature $>15^\circ\text{C}$ (Morita, 1975)), *A.*
424 *hydrophila* is a typical psychrotrophic microorganism capable of growth at 5°C (Grau, 1981).
425 We speculate that the adaptation to cold renders *A. hydrophila* strains expressing MARTX
426 toxin (Grim *et al.*, 2013, Tekedar *et al.*, 2013) less efficient towards humans than to fish and
427 amphibians, although immune-compromised people can still be infected by this pathogen
428 (Davis *et al.*, 1978). With the activity optimum steeply dropping around 37 - 40°C , ACD_{Ah} is
429 unlikely to be effective under the physiological conditions of human body. This correlates with
430 our unpublished observations that while being toxic to cultured mammalian cells under 37°C ,
431 *A. hydrophila* (strain ATCC 7566) does not cause any noticeable crosslinking of cytoplasmic
432 actin. It is tempting to speculate that the ability to tune the thermodynamic properties of the
433 adjacent effector domains by replacing/modifying its single element enables fast evolutionary
434 adaptation to new temperature conditions. Thus, low stability of ACD_{Ah} seems to extend to
435 other effector domains when in a fused state and is thereby likely to confer the efficient
436 translocation of these otherwise too rigid domains across the host membrane under cold
437 conditions. Yet, being cleaved off by CPD upon cytoplasmic delivery, ACD would not
438 undermine the stability of other effector domains under mesothermal conditions. This also
439 implies that the cellular effects of MARTX_{Ah} toxin might vary depending on temperature
440 conditions. In a broader context, it is tempting to speculate that the cassette type of a

441 synchronized delivery of several domains exploited in MARTX toxins not only allows
442 simultaneous delivery of several, often synergistic domains (e.g. ACD and RID), but may also
443 confer a remarkable flexibility in transportation of toxins that otherwise would be too rigid to
444 cross the membrane. To what degree this applies to different MARTX-based and other
445 cassette delivery mechanisms remains to be explored.

446 In agreement with the hypothesis that unfolding of MARTX effector domains occurs
447 under the human physiological conditions compatible with translocation across the host
448 membrane, fusion of the domains reduces precipitation and narrows the heterogeneity of
449 thermal transitions when compared to individual domain melting. The latter effect is
450 particularly prominent for the CPD-containing fusion proteins, all of which melt at
451 temperatures 10 - 23°C lower than the CPD domains alone (Table 1). Remarkably, $\Delta G^{\text{H}_2\text{O}}$ of
452 CPD_{Vc} is reduced 1.4 fold when the domain is fused to the adjacent ABH_{Vc} domain (Fig. 7A).
453 Melting properties of the CPD domains are noteworthy for several reasons. Thus, the CPD_{Vc}
454 domain is stable in the absence of a substrate (e.g. in the “post-cleavage” stage, when the
455 key recognition Leu residue is cleaved off (Prochazkova *et al.*, 2009) or simply not included in
456 the construct (this work)). However, it is substantially (by 11°C) destabilized upon interaction
457 with Leu of a substrate (e.g. when N-terminal Leu is included in the CPD sequence
458 (Prochazkova *et al.*, 2009) or when CPD is fused to other domains (this work)). Intriguingly,
459 Cys fluorescence probes (pyrene maleimide and acrylodan) destabilized CPD as revealed by
460 comparison of labeled and unlabeled CPDs’ $\Delta G^{\text{H}_2\text{O}}$ calculated based on Trp or
461 acrylodan/pyrene fluorescence upon urea denaturation (Fig. 7B). We believe that the
462 reduced CPD stability caused by modification of the catalytic cysteine may reflect the
463 mechanism of CPD destabilization by its substrate (adjacent effector domains). Indeed, the
464 Leu-containing region of the substrate also interacts with CPD in the catalytic region
465 (Prochazkova *et al.*, 2009) and might perturb the protein stability/conformation by affecting
466 the catalytic cysteine. We speculate that before cell entry, interaction with the substrate
467 destabilizes CPD and allows it to easily cross the membrane in an unfolded state. However, if
468 the same interaction happens inside the host cell, binding of InsP₆ stabilizes the structure
469 and activates the catalytic activity of CPD (Prochazkova *et al.*, 2009). Given the even higher
470 stability of CPD_{Ah} in the post-cleavage stage and its even greater destabilization when in
471 complex with other domains (Fig. 5 and 6; Table 1), the same general rules apply to both
472 CPD domains.

473 Overall, our data support the hypothesis that the effector domains of MARTX toxins are
474 transported across the cytoplasmic membrane in their partially or fully unfolded states. This
475 supposition is further indirectly supported by an obvious depletion of all known MARTX toxins
476 by cysteine residues. Thus, both ~0.5 MDa MARTX toxins from *V. cholerae* and *A.*
477 *hydrophila* have only two cysteine residues located in each of the CPD domains, as well as in
478 RID_{Vc} and MCF_{Ah} domains. Analysis of all twelve known MARTX toxins showed that effector
479 domains may contain from one (in CPD only) to a maximum of four cysteines. Under
480 oxidizing conditions of the extracellular environment, cysteines are prone to disulfide
481 crosslinking, which can efficiently prevent protein translocation through a narrow pore (Maher
482 & Singer, 1986). This strong evolutionary pressure applies only to unfolded proteins because
483 disulfide crosslinking can be efficiently evaded if the cysteines are hidden in the protein
484 interior, but it can hardly be avoided upon protein unfolding. Therefore, the only cysteines
485 that could not be negatively selected by evolution are those in the active sites of the
486 enzymes. Indeed, cysteine is essential for catalytic activity of CPD domains (Shen *et al.*,
487 2009, Prochazkova *et al.*, 2009), and it has been recently demonstrated that the catalytic
488 triad of RID domains also includes a cysteine (Ahrens *et al.*, 2013). The detailed molecular
489 mechanisms of the MCF apoptotic toxicity (Dowling *et al.*, 2007) are not known, but it can be
490 predicted that cysteine plays an important if not primary role in the activity of this protein as
491 well as in the catalytic function of most or all other Cys-containing MARTX effector domains.

492 The effector domains of the two MARTX toxins tested in the current study extend the list
493 of thermolabile, conformationally pliable bacterial toxins, suggesting that this quality is
494 essential for many pore-forming and membrane-penetrating toxins. As such, we propose that
495 thermodynamic instability can be utilized to create broad-spectrum antidotes for moderately
496 selective targeting and elimination of various classes of bacterial toxins. This type of antidote
497 can be particularly valuable for targeting infectious conditions when the causative agent/toxin
498 is unknown (e.g. in the case of emerging diseases or bioterrorist attacks). It appears also that
499 natural mechanisms targeting thermodynamic stability of bacterial toxins are already in place
500 in mammals and include hyperthermia and potentially humoral defense factors.

501

502 **EXPERIMENTAL PROCEDURES**

503 ***Recombinant protein expression and purification.*** DNA fragments encoding effector
504 domains of MARTX_{Vc} and MARTX_{Ah} were PCR-amplified from genomic DNA (gDNA) of the
505 *V. cholerae* N19691 strain (gDNA_{Vc} - generously donated by Dr. Satchell; Northwestern

506 University) and *A. hydrophila* (purified from ATCC 7966 cells using Axyprep Bacterial
507 Genomic DNA MiniPrep kit; Axygen). The amplified fragments encoding effector domains of
508 the toxins were cloned into the pCold I vector (Clontech) using In-fusion HD kit (Clontech). All
509 constructs were cloned in-frame with the N-terminal 6His-tag. Transformed BL21(DE3)pLysS
510 cells were grown in rich bacterial cell growth medium containing 1.25% tryptone, 2.5% yeast
511 extract, 125 mM NaCl, 0.4% glycerol, 50 mM Tris-HCl, pH 8.2 at 37°C. When the cells
512 reached OD₆₀₀=1-1.5, the induction of protein expression was achieved by cooling the culture
513 down to 15°C and adding 1 mM IPTG. Expression was carried out overnight at 15°C with 250
514 rpm agitation. Proteins were purified using TALON metal affinity resin (Clontech) according to
515 the manufacturer instructions. Briefly, cells were lysed by sonication in 50 mM phosphate
516 buffer, pH 7.5, containing 300 mM NaCl, 5 mM imidazole, 10 mM PMSF, and protease
517 inhibitor cocktail (Sigma). The cell lysates were clarified by centrifugation (30 min at 90,000 g
518 at 4°C) and applied to TALON column. Unbound material was removed by washing the
519 column with the lysis buffer containing 10-20 mM imidazole. Elution of 6His-tagged proteins
520 was achieved with the lysis buffer containing 50-250 mM imidazole. Proteins were
521 concentrated using Amicon centrifugal filters and dialysed either in 20 mM Tris, pH 7.5, 150
522 mM NaCl, 0.1 mM PMSF or 50 mM phosphate buffer, pH 7.5, 0.1 mM PMSF; aliquots were
523 flash frozen in liquid nitrogen and stored at -80°C.

524 Bacterial cell strains, plasmid DNA, and primer sequences used in this study are
525 presented in Table S1. Information about the recombinant proteins cloned, expressed, and
526 purified in the present study is summarized in Table 1. SDS-PAGE of purified proteins is
527 shown in Fig. 1B. We were unable to purify MCF_{Ah} domain in its native state as it was
528 insoluble. Five-domain MARTX_{Ah} fusion protein was purified in the presence of N-
529 ethylmaleimide, which helped to protect it from degradation. Activities of ACD and CPD were
530 monitored to ensure proper protein folding of the constructs (Fig. 1C,D). Conditions for actin
531 crosslinking activity of ACD are described below. Protease activity of CPD and
532 autoprocessing activity of CPD-containing constructs were assessed in 20 mM Tris-HCl, pH
533 7.5, 150 mM NaCl after the addition of 0.1 mM InsP₆ for 90 min and analyzed by SDS-PAGE.

534 **Actin purification.** Skeletal muscle actin was prepared from acetone powder from rabbit
535 skeletal muscles (Pel-Freez Biologicals) as described (Spudich & Watt, 1971) and stored in
536 G-buffer (5.0 mM TRIS, pH 8.0, 0.2 mM Ca²⁺-ATP, 5.0 mM β-mercaptoethanol) on ice for 2
537 weeks or flash frozen in liquid nitrogen for prolonged storage.

538 **Temperature dependence of ACD activity.** ACD-catalyzed crosslinking was performed

539 in a reaction buffer containing 2.0 mM MgCl₂, 0.2 mM EGTA, 0.5 mM ATP, 10 mM HEPES,
540 pH 7.5 as described previously (Kudryashova *et al.*, 2012). Briefly, actin was pre-incubated
541 with 1.5 molar excess of latrunculin B (Enzo Life Sciences) for 15 minutes to prevent actin
542 polymerization and crosslinking was initiated by addition of MgCl₂ (2.0 mM) to a mixture of
543 actin and ACD (500-250:1 molar ratio of ACD to actin) in the reaction buffer lacking MgCl₂.
544 Reactions were incubated at corresponding temperatures and the crosslinking was stopped
545 within 1 - 3 minutes of initiation by adding SDS-PAGE sample buffer and boiling. Crosslinked
546 actin species were resolved on 7.5% SDS-gels and stained with Coomassie Brilliant Blue R-
547 250. Images were obtained using Perfection V600 EPSON scanner. Densitometry was
548 performed using ImageJ image-processing software (<http://rsb.info.nih.gov/ij/>). The rates of
549 ACD activity were expressed in percent of the maximum activity of the enzyme.

550 ***Intrinsic fluorescence measurements.*** Fluorescence emission spectra of protein
551 denaturation induced by GdnHCl and urea were recorded using multifunctional plate-reader
552 Infinite-M1000 Pro (Tecan). Excitation wavelength was set to 295 nm; excitation and
553 emission slits were 2.5 and 5 nm, respectively. 5 μM of the sample protein in phosphate
554 buffered saline (PBS: 137 mM NaCl, 2.7 mM KCl, 10 mM Na₂HPO₄, and 2 mM KH₂PO₄, pH
555 7.4) was mixed with increasing concentrations of GdnHCl (0 - 4 M) or urea (0 - 6 M) and
556 incubated for 1 h at room temperature (23°C) to attain equilibrium before measurements. The
557 maximum wavelength of emission (λ_{\max}) was determined and the data were analyzed
558 according to the two-state transition model (Pace, 1986, Greene & Pace, 1974).

559 Assuming a two-state transition model, free energy change of ACD_{vc} unfolding for a
560 given denaturant concentration (ΔG) was calculated using the equation (1):

561
$$\Delta G = -R \times T \times \ln K \quad (1),$$

562 where R is the universal gas constant, T is temperature in Kelvin; K is the equilibrium
563 constant, which was calculated from the equation (2):

564
$$K = ((y_U F - y)) / (([y - y_U] U)) \quad (2),$$

565 where y is the observed λ_{\max} at different concentrations of denaturant, and y_F and y_U are the
566 λ_{\max} for the folded (F) and unfolded (U) conformations of the protein, respectively (Pace,
567 1986). ΔG was plotted as a function of denaturant concentration and a linear extrapolation to
568 zero denaturant concentration was applied to calculate free energy difference of unfolding in
569 the absence of denaturant ($\Delta G^{\text{H}_2\text{O}}$) using the equation (3) (Greene & Pace, 1974):

570
$$\Delta G = \Delta G^{H_2O} + m \times [GdnHCl] \quad (3),$$

571 where m is a slope term, which determines the change in ΔG per unit concentration of
 572 denaturant [GdnHCl] or [urea]. The transition midpoint corresponding to denaturant
 573 concentration at which 50% of a protein is in the unfolded state $[\text{denaturant}]_{1/2}$ was
 574 determined according to the equation (4):

575
$$[\text{denaturant}]_{1/2} = \frac{\Delta G^{H_2O}}{m} \quad (4).$$

576 Data were fit to equation (5) using Kaleidagraph software:

577
$$L = \frac{((L_u + m_u \times [D]) + (L_f + m_f \times [D])) \times e^{\frac{-(\Delta G^{H_2O} + m \times [D])}{RT}}}{1 + e^{\frac{-(\Delta G^{H_2O} + m \times [D])}{RT}}} \quad (5),$$

578 where L – wavelength maximum, $[D]$ – denaturant concentration, L_f and L_u – wavelength
 579 maximums of folded and unfolded states respectively, m_f and m_u are slopes of pre- and post-
 580 transition baselines, ΔG^{H_2O} - free energy change of unfolding in the absence of denaturant,
 581 and factor m is a slope term, which determines the change in ΔG per unit concentration of
 582 denaturant.

583 **Fluorescent labeling of Cys residue in the active site of CPD_{Vc}.** CPD_{Vc} was
 584 incubated in the presence of 1 mM TCEP for 1 hour and the reducing agent was removed by
 585 passing the protein through Zeba column (Pierce) equilibrated with PBS. 1.5 molar excess of
 586 acrylodan or pyrene maleimide (Life Technologies) were added and the labeling proceeded
 587 for 4 hours followed by free dye removal by Zeba column. Acrylodan and pyrene
 588 fluorescence of 1 μM labeled CPD_{Vc} was monitored using multifunctional plate-reader
 589 Infinite-M1000 Pro (Tecan). Excitation wavelength was set to 391 nm for acrylodan and 340
 590 nm for pyrene; excitation and emission slits were set to 5 nm. Urea-induced CPD_{Vc} unfolding
 591 was detected as a shift in acrylodan emission wavelength maximum or a decrease of pyrene
 592 fluorescence intensity at 374 nm (Fig. S10).

593 **CD spectroscopy.** Far- and near-UV CD spectra were obtained using JASCO J-815 CD
 594 instrument (JASCO Analytical Instruments) equipped with a Peltier temperature controller.
 595 Quartz cuvettes with 0.1 and 1 cm length path were used for far- and near-UV CD,
 596 respectively. All proteins were dialyzed against 50 mM sodium phosphate buffer, pH 7.4. The
 597 protein concentration was determined by the Edelhoch method (Edelhoch, 1967). The
 598 concentrations of the samples were adjusted to 0.5 mg/ml for both far- and near-UV CD.

599 Each wavelength scan was obtained as an average of three accumulations after background
 600 subtraction. Temperature denaturation curves (CD signals at a specific wavelength as a
 601 function of temperature) and corresponding dynode voltages were recorded over a range of
 602 temperatures at a rate 2°C per minute every 1°C. A slower rate of 1°C/min yielded similar
 603 results (data not shown). Apparent T_m values of protein secondary structure unfolding were
 604 determined as far-UV CD transition midpoints. Additionally, entire spectra of far- and near-UV
 605 CD signals for ACD_{vc} were collected at certain temperatures during ramping between 20 and
 606 80°C, at a scanning speed 100 nm/min, using 1 and 2 nm bandwidths for far- and near-UV
 607 CD, respectively. Far-UV CD signals were expressed as the mean residue molar ellipticity:

$$608 \quad [\theta] = \frac{\theta \times 100 \times M}{C \times l \times n} \quad (6),$$

609 where Θ is the ellipticity (degrees), l - optical path (cm), C - concentration (mg/ml), M -
 610 molecular mass, n - the number of amino acid residues. Near-UV CD signals were expressed
 611 as the molar circular dichroism (Kelly & Price, 1997):

$$612 \quad \Delta\varepsilon = \frac{[\theta]}{3298.2} \quad (7).$$

613 **Differential scanning fluorimetry (DSF).** Temperature denaturation curves in the
 614 presence of SYPRO Orange dye (Invitrogen) were obtained using CFX96 Touch Real-Time
 615 PCR Detection System (Bio-Rad). The proteins were diluted in phosphate buffered saline (pH
 616 7.4) to 10 - 20 μ M. The dye was used at 1 x concentration (molar concentration of SYPRO
 617 Orange is proprietary information of Invitrogen). Temperature was increased at a rate 2°C per
 618 minute and fluorescent signal was recorded every 1°C. DSF fluorescence intensity was
 619 plotted as a function of temperature, which generates a two-state transition sigmoidal curve.
 620 Therefore, a variation of Boltzmann equation is generally applied to fit the DSF data and to
 621 calculate the inflection point of the transition (T_m) (Niesen *et al.*, 2007):

$$622 \quad F = F_f + \frac{(F_u - F_f) + e^{\frac{T_m - T}{a}}}{1 + e^{\frac{T_m - T}{a}}} \quad (8),$$

623 where F is fluorescence signal, F_f and F_u - fluorescence of folded and unfolded states
 624 respectively, T - temperature, T_m - melting temperature, and factor a is related to the slope
 625 of the transition within T_m . To account for non-flat pre- and post-transition baselines
 626 according to Clarke and Fersht (Clarke & Fersht, 1993):

$$627 \quad F_f = \alpha_f + [(\beta)_f \times T] \quad \text{and} \quad F_u = \alpha_u + [(\beta)_u \times T] \quad (9) \text{ and } (10),$$

628 where α_f and β_f are intercept and slope of pre-transition baseline, α_u and β_u are intercept and
629 slope of post-transition baseline. To calculate the DSF T_m values, the DSF data were fit using
630 Kaleidagraph software to the modified Boltzman equation:

$$F = (\alpha_f + \beta_f \times T) + \frac{((\alpha_u + \beta_u \times T) - (\alpha_f + \beta_f \times T)) + e^{\frac{T_m - T}{a}}}{1 + e^{\frac{T_m - T}{a}}}$$

631
632 (11).

633 The values of α_f , β_f , α_u , and β_u were fit from the fluorescence signals at temperatures T in pre-
634 and post-transition regions by least-squares using Microsoft Excel; a – an exponential factor
635 dependent on the slope of the transition at the apparent T_m (Table S2).

636 **Statistical analysis.** Data were analyzed using Microsoft Excel software. Average
637 values were obtained from 3 independent experiments. Errors represent standard errors of
638 mean values. Statistical significance was determined by two-tailed Student's t-test ($p < 0.05$).

639

640 ACKNOWLEDGEMENTS

641 We thank Dr. Karla Satchell (Northwestern University) for a generous gift of gDNA from *V.*
642 *cholerae* and Dr. Irina Artsimovitch (The Ohio State University) for providing access to a real-
643 time PCR instrument. This work was partially supported by American Heart Association
644 Innovative Research Grant 13IRG14780028 to DK.

645

646 Conflict of interest

647 The authors declare no conflict of interest.

648

649 REFERENCES

- 650 Ahrens, S., B. Geissler & K.J. Satchell, (2013) Identification of a His-Asp-Cys catalytic triad
651 essential for function of the Rho inactivation domain (RID) of *Vibrio cholerae* MARTX
652 toxin. *J Biol Chem* **288**: 1397-1408.
- 653 Benjwal, S., S. Verma, K.H. Rohm & O. Gursky, (2006) Monitoring protein aggregation during
654 thermal unfolding in circular dichroism experiments. *Protein Sci* **15**: 635-639.
- 655 Bychkova, V.E., A.E. Dujsekina, A. Fantuzzi, O.B. Ptitsyn & G.L. Rossi, (1998) Release of
656 retinol and denaturation of its plasma carrier, retinol-binding protein. *Fold Des* **3**: 285-
657 291.
- 658 Cai, S., R. Kukreja, S. Shoosmith, T.W. Chang & B.R. Singh, (2006) Botulinum neurotoxin
659 light chain refolds at endosomal pH for its translocation. *Protein J* **25**: 455-462.

- 660 Clarke, J. & A.R. Fersht, (1993) Engineered disulfide bonds as probes of the folding pathway
661 of barnase: increasing the stability of proteins against the rate of denaturation.
662 *Biochemistry* **32**: 4322-4329.
- 663 Cordero, C.L., D.S. Kudryashov, E. Reisler & K.J. Satchell, (2006) The Actin cross-linking
664 domain of the *Vibrio cholerae* RTX toxin directly catalyzes the covalent cross-linking
665 of actin. *J Biol Chem* **281**: 32366-32374.
- 666 Davis, W.A., 2nd, J.G. Kane & V.F. Garagusi, (1978) Human aeromonas infections: a review
667 of the literature and a case report of endocarditis. *Medicine (Baltimore)* **57**: 267-277.
- 668 Dowling, A.J., N.R. Waterfield, M.C. Hares, G. Le Goff, C.H. Streuli & R.H. French-Constant,
669 (2007) The Mcf1 toxin induces apoptosis via the mitochondrial pathway and apoptosis
670 is attenuated by mutation of the BH3-like domain. *Cell Microbiol* **9**: 2470-2484.
- 671 Durand, E., E. Derrez, G. Audoly, S. Spinelli, M. Ortiz-Lombardia, D. Raoult, E. Cascales &
672 C. Cambillau, (2012) Crystal structure of the VgrG1 actin cross-linking domain of the
673 *Vibrio cholerae* type VI secretion system. *J Biol Chem* **287**: 38190-38199.
- 674 Edelhoch, H., (1967) Spectroscopic determination of tryptophan and tyrosine in proteins.
675 *Biochemistry* **6**: 1948-1954.
- 676 Egerer, M. & K.J. Satchell, (2010) Inositol hexakisphosphate-induced autoprocessing of large
677 bacterial protein toxins. *PLoS Pathog* **6**: e1000942.
- 678 Feld, G.K., K.L. Thoren, A.F. Kintzer, H.J. Sterling, Tang, II, S.G. Greenberg, E.R. Williams &
679 B.A. Krantz, (2010) Structural basis for the unfolding of anthrax lethal factor by
680 protective antigen oligomers. *Nat Struct Mol Biol* **17**: 1383-1390.
- 681 Feller, G., (2010) Protein stability and enzyme activity at extreme biological temperatures. *J*
682 *Phys Condens Matter* **22**: 323101.
- 683 Feller, G. & C. Gerday, (2003) Psychrophilic enzymes: hot topics in cold adaptation. *Nat Rev*
684 *Microbiol* **1**: 200-208.
- 685 Fullner, K.J. & J.J. Mekalanos, (2000) In vivo covalent cross-linking of cellular actin by the
686 *Vibrio cholerae* RTX toxin. *EMBO J* **19**: 5315-5323.
- 687 Grau, F.H., (1981) Role of pH, lactate, and anaerobiosis in controlling the growth of some
688 fermentative Gram-negative bacteria on beef. *Appl Environ Microbiol* **42**: 1043-1050.
- 689 Greene, R.F., Jr. & C.N. Pace, (1974) Urea and guanidine hydrochloride denaturation of
690 ribonuclease, lysozyme, alpha-chymotrypsin, and beta-lactoglobulin. *J Biol Chem*
691 **249**: 5388-5393.
- 692 Grim, C.J., E.V. Kozlova, J. Sha, E.C. Fitts, C.J. van Lier, M.L. Kirtley, S.J. Joseph, T.D.
693 Read, E.M. Burd, B.D. Tall, S.W. Joseph, A.J. Horneman, A.K. Chopra & J.R. Shak,
694 (2013) Characterization of *Aeromonas hydrophila* wound pathotypes by comparative
695 genomic and functional analyses of virulence genes. *MBio* **4**: e00064-00013.
- 696 Gupta, P., S. Singh, A. Tiwari, R. Bhat & R. Bhatnagar, (2001) Effect of pH on stability of
697 anthrax lethal factor: correlation between denaturation and activity. *Biochem Biophys*
698 *Res Commun* **284**: 568-573.
- 699 Hasani, L., B. Ranjbar, M. Tavallaie & M. Sadeghizadeh, (2009) Identification of a molten
700 globule like state in HC-N fragment of botulinum neurotoxin A: shedding light on the
701 poorly-known features of a conserved sub-domain. *Protein Pept Lett* **16**: 660-663.
- 702 Herlax, V. & L. Bakas, (2007) Fatty acids covalently bound to alpha-hemolysin of *Escherichia*
703 *coli* are involved in the molten globule conformation: implication of disordered regions
704 in binding promiscuity. *Biochemistry* **46**: 5177-5184.
- 705 Kelly, S.M. & N.C. Price, (1997) The application of circular dichroism to studies of protein
706 folding and unfolding. *Biochim Biophys Acta* **1338**: 161-185.
- 707 Kelly, S.M. & N.C. Price, (2000) The use of circular dichroism in the investigation of protein
708 structure and function. *Curr Protein Pept Sci* **1**: 349-384.

- 709 Kim, Y.R., S.E. Lee, H. Kook, J.A. Yeom, H.S. Na, S.Y. Kim, S.S. Chung, H.E. Choy & J.H.
710 Rhee, (2008) *Vibrio vulnificus* RTX toxin kills host cells only after contact of the
711 bacteria with host cells. *Cell Microbiol* **10**: 848-862.
- 712 Krantz, B.A., A. Finkelstein & R.J. Collier, (2006) Protein translocation through the anthrax
713 toxin transmembrane pore is driven by a proton gradient. *J Mol Biol* **355**: 968-979.
- 714 Krantz, B.A., A.D. Trivedi, K. Cunningham, K.A. Christensen & R.J. Collier, (2004) Acid-
715 induced unfolding of the amino-terminal domains of the lethal and edema factors of
716 anthrax toxin. *J Mol Biol* **344**: 739-756.
- 717 Kudryashov, D.S., C.L. Cordero, E. Reisler & K.J. Satchell, (2008a) Characterization of the
718 enzymatic activity of the actin cross-linking domain from the *Vibrio cholerae* MARTX
719 Vc toxin. *J Biol Chem* **283**: 445-452.
- 720 Kudryashov, D.S., Z.A. Durer, A.J. Ytterberg, M.R. Sawaya, I. Pashkov, K. Prochazkova,
721 T.O. Yeates, R.R. Loo, J.A. Loo, K.J. Satchell & E. Reisler, (2008b) Connecting actin
722 monomers by iso-peptide bond is a toxicity mechanism of the *Vibrio cholerae* MARTX
723 toxin. *Proc Natl Acad Sci U S A* **105**: 18537-18542.
- 724 Kudryashova, E., C. Kalda & D.S. Kudryashov, (2012) Glutamyl phosphate is an activated
725 intermediate in actin crosslinking by actin crosslinking domain (ACD) toxin. *PLoS One*
726 **7**: e45721.
- 727 Kwak, J.S., H.G. Jeong & K.J. Satchell, (2011) *Vibrio vulnificus* rtxA1 gene recombination
728 generates toxin variants with altered potency during intestinal infection. *Proc Natl*
729 *Acad Sci U S A* **108**: 1645-1650.
- 730 Lakey, J.H., J.M. Gonzalez-Manas, F.G. van der Goot & F. Pattus, (1992) The membrane
731 insertion of colicins. *FEBS Lett* **307**: 26-29.
- 732 Lally, E.T., R.B. Hill, I.R. Kieba & J. Korostoff, (1999) The interaction between RTX toxins
733 and target cells. *Trends Microbiol* **7**: 356-361.
- 734 Lee, B.C., J.H. Lee, M.W. Kim, B.S. Kim, M.H. Oh, K.S. Kim, T.S. Kim & S.H. Choi, (2008)
735 *Vibrio vulnificus* rtxE is important for virulence, and its expression is induced by
736 exposure to host cells. *Infect Immun* **76**: 1509-1517.
- 737 Lee, P.A., D. Tullman-Ercek & G. Georgiou, (2006) The bacterial twin-arginine translocation
738 pathway. *Annu Rev Microbiol* **60**: 373-395.
- 739 Louis-Jeune, C., M.A. Andrade-Navarro & C. Perez-Iratxeta, (2011) Prediction of protein
740 secondary structure from circular dichroism using theoretically derived spectra.
741 *Proteins* **80**: 374-381.
- 742 Maher, P.A. & S.J. Singer, (1986) Disulfide bonds and the translocation of proteins across
743 membranes. *Proc Natl Acad Sci U S A* **83**: 9001-9005.
- 744 Miller, C.J., B.S. Drasar & R.G. Feachem, (1984) Response of toxigenic *Vibrio cholerae* 01 to
745 physico-chemical stresses in aquatic environments. *J Hyg (Lond)* **93**: 475-495.
- 746 Morita, R.Y., (1975) Psychrophilic bacteria. *Bacteriol Rev* **39**: 144-167.
- 747 Niesen, F.H., H. Berglund & M. Vedadi, (2007) The use of differential scanning fluorimetry to
748 detect ligand interactions that promote protein stability. *Nat Protoc* **2**: 2212-2221.
- 749 Ohgushi, M. & A. Wada, (1983) 'Molten-globule state': a compact form of globular proteins
750 with mobile side-chains. *FEBS Lett* **164**: 21-24.
- 751 Pace, C.N., (1986) Determination and analysis of urea and guanidine hydrochloride
752 denaturation curves. *Methods Enzymol* **131**: 266-280.
- 753 Pande, A.H., P. Scaglione, M. Taylor, K.N. Nemecek, S. Tuthill, D. Moe, R.K. Holmes, S.A.
754 Tatulian & K. Teter, (2007) Conformational instability of the cholera toxin A1
755 polypeptide. *J Mol Biol* **374**: 1114-1128.
- 756 Park, C. & S. Marqusee, (2004) Analysis of the stability of multimeric proteins by effective
757 DeltaG and effective m-values. *Protein Sci* **13**: 2553-2558.

- 758 Pei, J. & N.V. Grishin, (2009) The Rho GTPase inactivation domain in *Vibrio cholerae*
759 MARTX toxin has a circularly permuted papain-like thiol protease fold. *Proteins* **77**:
760 413-419.
- 761 Prochazkova, K. & K.J. Satchell, (2008) Structure-function analysis of inositol
762 hexakisphosphate-induced autoprocessing of the *Vibrio cholerae* multifunctional
763 autoprocessing RTX toxin. *J Biol Chem* **283**: 23656-23664.
- 764 Prochazkova, K., L.A. Shuvalova, G. Minasov, Z. Voburka, W.F. Anderson & K.J. Satchell,
765 (2009) Structural and molecular mechanism for autoprocessing of MARTX toxin of
766 *Vibrio cholerae* at multiple sites. *J Biol Chem* **284**: 26557-26568.
- 767 Queen, J. & K.J. Satchell, (2012) Neutrophils are essential for containment of *Vibrio cholerae*
768 to the intestine during the proinflammatory phase of infection. *Infect Immun* **80**: 2905-
769 2913.
- 770 Ren, J., J.C. Sharpe, R.J. Collier & E. London, (1999) Membrane translocation of charged
771 residues at the tips of hydrophobic helices in the T domain of diphtheria toxin.
772 *Biochemistry* **38**: 976-984.
- 773 Roig, F.J., F. Gonzalez-Candelas & C. Amaro, (2011) Domain organization and evolution of
774 multifunctional autoprocessing repeats-in-toxin (MARTX) toxin in *Vibrio vulnificus*.
775 *Appl Environ Microbiol* **77**: 657-668.
- 776 Salnikova, M.S., S.B. Joshi, J.H. Rytting, M. Warny & C.R. Middaugh, (2008) Physical
777 characterization of *Clostridium difficile* toxins and toxoids: effect of the formaldehyde
778 crosslinking on thermal stability. *J Pharm Sci* **97**: 3735-3752.
- 779 Satchell, K.J., (2007) MARTX, multifunctional autoprocessing repeats-in-toxin toxins. *Infect*
780 *Immun* **75**: 5079-5084.
- 781 Satchell, K.J., (2011) Structure and function of MARTX toxins and other large repetitive RTX
782 proteins. *Annu Rev Microbiol* **65**: 71-90.
- 783 Schuerch, D.W., E.M. Wilson-Kubalek & R.K. Tweten, (2005) Molecular basis of listeriolysin
784 O pH dependence. *Proc Natl Acad Sci U S A* **102**: 12537-12542.
- 785 Sheahan, K.L., C.L. Cordero & K.J. Satchell, (2004) Identification of a domain within the
786 multifunctional *Vibrio cholerae* RTX toxin that covalently cross-links actin. *Proc Natl*
787 *Acad Sci U S A* **101**: 9798-9803.
- 788 Sheahan, K.L. & K.J. Satchell, (2007) Inactivation of small Rho GTPases by the
789 multifunctional RTX toxin from *Vibrio cholerae*. *Cell Microbiol* **9**: 1324-1335.
- 790 Shen, A., P.J. Lupardus, V.E. Albrow, A. Guzzetta, J.C. Powers, K.C. Garcia & M. Bogyo,
791 (2009) Mechanistic and structural insights into the proteolytic activation of *Vibrio*
792 *cholerae* MARTX toxin. *Nat Chem Biol* **5**: 469-478.
- 793 Somero, G.N., (1995) Proteins and temperature. *Annu Rev Physiol* **57**: 43-68.
- 794 Spudich, J.A. & S. Watt, (1971) The regulation of rabbit skeletal muscle contraction. I.
795 Biochemical studies of the interaction of the tropomyosin-troponin complex with actin
796 and the proteolytic fragments of myosin. *J Biol Chem* **246**: 4866-4871.
- 797 Tekedar, H.C., G.C. Waldbieser, A. Karsi, M.R. Liles, M.J. Griffin, S. Vamenta, T.
798 Sonstegard, M. Hossain, S.G. Schroeder, L. Khoo & M.L. Lawrence, (2013) Complete
799 Genome Sequence of a Channel Catfish Epidemic Isolate, *Aeromonas hydrophila*
800 Strain ML09-119. *Genome Announc* **1**(5): e00755-13.
- 801 Thoren, K.L., E.J. Worden, J.M. Yassif & B.A. Krantz, (2009) Lethal factor unfolding is the
802 most force-dependent step of anthrax toxin translocation. *Proc Natl Acad Sci U S A*
803 **106**: 21555-21560.
- 804 van der Goot, F.G., J.M. Gonzalez-Manas, J.H. Lakey & F. Pattus, (1991) A 'molten-globule'
805 membrane-insertion intermediate of the pore-forming domain of colicin A. *Nature* **354**:
806 408-410.

807 Wynia-Smith, S.L., M.J. Brown, G. Chirichella, G. Kemalyan & B.A. Krantz, (2012)
808 Electrostatic ratchet in the protective antigen channel promotes anthrax toxin
809 translocation. *J Biol Chem* **287**: 43753-43764.
810 Zhao, J.M. & E. London, (1986) Similarity of the conformation of diphtheria toxin at high
811 temperature to that in the membrane-penetrating low-pH state. *Proc Natl Acad Sci U*
812 *S A* **83**: 2002-2006.
813

814

815

816 **FIGURE LEGENDS**

817 **Figure 1. Domain structure of MARTX_{Vc} and MARTX_{Ah}.** (A) Schematic diagrams of
818 MARTX_{Vc} and MARTX_{Ah} toxins: conserved repeats (A1, A2, B, and C) and effector domains
819 are shown in scale. (B) SDS-PAGE of purified recombinant domains of MARTX toxins. ACD
820 – actin crosslinking domain, ABH – α/β hydrolase, PMT – similar to *Pasteurella multocida*
821 toxin, RID – Rho-GTPase inactivation domain, CPD – cysteine protease domain. Multi-
822 domain constructs are numbered as follows: 1 - ACD-ABH_{Ah}, 2 - MCF-PMT_{Ah}, 3 - PMT-
823 CPD_{Ah}, 4 - ACD-ABH-MCF-PMT_{Ah}, 5 - ACD-ABH-MCF-PMT-CPD_{Ah}, 6 - ACD-RID_{Vc}, 7 - RID-
824 ABH_{Vc}, 8 - ABH-CPD_{Vc}, 9 - ACD-RID-ABH_{Vc}, 10 - ACD-RID-ABH-CPD_{Vc}. Additional minor 40
825 kDa band in lane 8 is a result of residual activity of CPD_{Vc} (as seen on Fig. 1D(3)). Loading –
826 5 μ g of protein per well. (C, D) Activity assays were carried out for ACD- and CPD-containing
827 recombinant constructs to ensure their proper folding. (C) Actin-crosslinking was carried out
828 for 30 min at room temperature in the presence of ACD_{Vc} (lane 2), ACD-RID_{Vc} (lane 3), ACD-
829 RID-ABH_{Vc} (lane 4), ACD-RID-ABH-CPD_{Vc} (lane 5) at a molar ratio to actin 1:500. M – MW
830 ladder; lane 1 – actin alone. (D) Protease activity of CPD was verified for CPD_{Vc}, ACD-RID-
831 ABH-CPD_{Vc}, and ABH-CPD_{Vc}. Reactions were initiated by addition of 0.1 mM InsP₆. 1 –
832 CPD_{Vc} was incubated in the presence of its substrate ACD-RID-ABH_{Vc}; 2 and 3 – self-
833 cleavage of ACD-RID-ABH-CPD_{Vc} and ABH-CPD_{Vc}, respectively. Final concentrations of
834 proteins were 0.1 mg/ml for CPD_{Vc} and 0.5 mg/ml for all other constructs. Resulting cleavage
835 products are indicated at right based on their molecular weights (MW is shown in
836 parenthesis); 4d (185) - ACD-RID-ABH-CPD_{Vc} (185 kDa), 3d (163) - ACD-RID-ABH_{Vc} (163
837 kDa), 2d (126) - ACD-RID_{Vc} (126 kDa), 2d (111) - RID-ABH_{Vc} (111 kDa).

838 **Figure 2. Temperature dependence of ACD activity.** (A) Actin crosslinking by ACD_{Ah}
839 and ACD_{Vc} at different temperatures was monitored by SDS-PAGE. (B) Relative ACD activity

840 (% of maximum) was plotted as a function of temperature. Error bars represent standard
841 errors of means; $n = 3$.

842 **Figure 3. Chemically induced denaturation of ACD_{Vc}.** Intrinsic Trp fluorescence
843 during chemically induced unfolding of ACD_{Vc} was monitored in the presence of increasing
844 concentrations of GdnHCl (A) or urea (B). λ_{\max} was plotted against concentration of the
845 denaturants. Inserts show plots of free energy changes of ACD_{Vc} unfolding (ΔG) for a given
846 denaturant concentration, [GdnHCl] or [Urea]. Parameters obtained from fitting the data to
847 the equation 5 for GdnHCl denaturation: $\Delta G^{\text{H}_2\text{O}}=2.75\pm 0.14$ kcal/mol (11.5 kJ/mol),
848 $m=3.16\pm 0.17$ kcal/mol/M, $[\text{GdnHCl}]_{1/2}=0.87$ M; for urea denaturation: $\Delta G^{\text{H}_2\text{O}}=2.72\pm 0.11$
849 kcal/mol (11.4 kJ/mol), $m=1.63\pm 0.07$ kcal/mol/M, $[\text{urea}]_{1/2}=1.67$ M.

850 **Figure 4. Thermal unfolding of ACD_{Vc} as revealed by CD.** Thermal unfolding of
851 secondary and tertiary structures of ACD_{Vc} was monitored by far- (A, B) and near-UV (C, D)
852 CD spectroscopy. Entire CD spectra were obtained at different temperatures as indicated on
853 figures (A) and (C). CD signals at a specific wavelength were recorded as functions of
854 temperature: 208 nm for far-UV CD (B) and 290 nm for near-UV CD (D). Dynode voltage
855 (black lines in (B) and (D)) was routinely monitored as a measure of protein aggregation.
856 Note two transition steps for near-UV CD temperature dependence (C, D). Leveling of the
857 ACD_{Vc} characteristic minima at 290 and 283 nm reflects rearrangements in the environment
858 of tertiary structure elements at $<46^\circ\text{C}$ (#1 in C and D). The drop of signal (#2 in C and D)
859 coincides with precipitation at $>46^\circ\text{C}$ as seen by concurrent dramatic increase of dynode
860 voltage (D).

861 **Figure 5. Thermal unfolding of the effector domains and CPD from MARTX_{Vc} and**
862 **MARTX_{Ah} toxins as monitored by CD.** Far-UV CD signals of individual (A, B) or fused (C,
863 D) MARTX domains of *V. cholerae* (A, C) or *A. hydrophila* (B, D) were recorded as functions
864 of temperature. Signals were normalized for each recombinant protein with the highest in the
865 transition region expressed as 1 and the lowest set as 0. Apparent half-transition points are
866 shown with dotted lines.

867 **Figure 6. Thermal unfolding of the effector domains and CPD from MARTX_{Vc} and**
868 **MARTX_{Ah} toxins as monitored by DSF.** DSF signals of individual (A, B) or fused (C, D)
869 MARTX domains of *V. cholerae* (A, C) or *A. hydrophila* (B, D) were recorded as functions of
870 temperature and normalized for each recombinant protein with the highest signal in the
871 transition region expressed as 1 and the lowest signal set as 0. Half-transition points are
872 shown with dotted lines.

873 **Figure 7. Destabilization of CPD_{VC} by fusion with the adjacent domain and by**
874 **Cys-labeling.** (A) Trp fluorescence of CPD_{VC} was monitored during denaturation of CPD_{VC}
875 (closed circles) or ABH-CPD_{VC} (open circles) with urea. Parameters obtained from fitting the
876 data to equation 5 for CPD_{VC} in separation: $\Delta G^{\text{H}_2\text{O}}=5.22\pm 0.56$ kcal/mol (21.84 kJ/mol),
877 $m=2.37\pm 0.35$ kcal/mol/M, $[\text{urea}]_{1/2}=2.2$ M; for CPD_{VC} fused to ABH_{VC}: $\Delta G^{\text{H}_2\text{O}}=3.84\pm 0.5$
878 kcal/mol (16.07 kJ/mol), $m=2.23\pm 0.27$ kcal/mol/M, $[\text{urea}]_{1/2}=1.72$ M. (B) CPD_{VC} was labeled
879 with acrylodan or pyrene maleimide and its unfolding in urea was monitored by changes in
880 the corresponding fluorescence signals. Additionally, Trp fluorescence was recorded for
881 unlabeled or acrylodan-labeled CPD_{VC}. Fraction of unfolded protein was calculated and
882 plotted against urea concentration. Parameters obtained from fitting the data to equation 5
883 are as followed: 1) unlabeled CPD_{VC} (Trp fluorescence; closed black circles):
884 $\Delta G^{\text{H}_2\text{O}}=5.22\pm 0.56$ kcal/mol (21.84 kJ/mol), $m=2.37\pm 0.35$ kcal/mol/M, $[\text{urea}]_{1/2}=2.2$ M; 2)
885 acrylodan-labeled CPD_{VC} (Trp fluorescence; open black circles): $\Delta G^{\text{H}_2\text{O}}=2.78\pm 0.34$ kcal/mol
886 (11.6 kJ/mol), $m=2.06\pm 0.29$ kcal/mol/M, $[\text{urea}]_{1/2}=1.35$ M; 3) acrylodan-labeled CPD_{VC}
887 (acrylodan fluorescence; gray triangles): $\Delta G^{\text{H}_2\text{O}}=3.07\pm 0.11$ kcal/mol (12.8 kJ/mol),
888 $m=2.06\pm 0.08$ kcal/mol/M, $[\text{urea}]_{1/2}=1.49$ M; 4) pyrene-labeled CPD_{VC} (pyrene fluorescence;
889 gray squares): $\Delta G^{\text{H}_2\text{O}}=2.38\pm 0.12$ kcal/mol (9.96 kJ/mol), $m=1.71\pm 0.09$ kcal/mol/M,
890 $[\text{urea}]_{1/2}=1.39$ M.

891

892

893 **Table 1. Recombinant effector domains of MARTX_{Vc} and MARTX_{Ah} toxins**

894

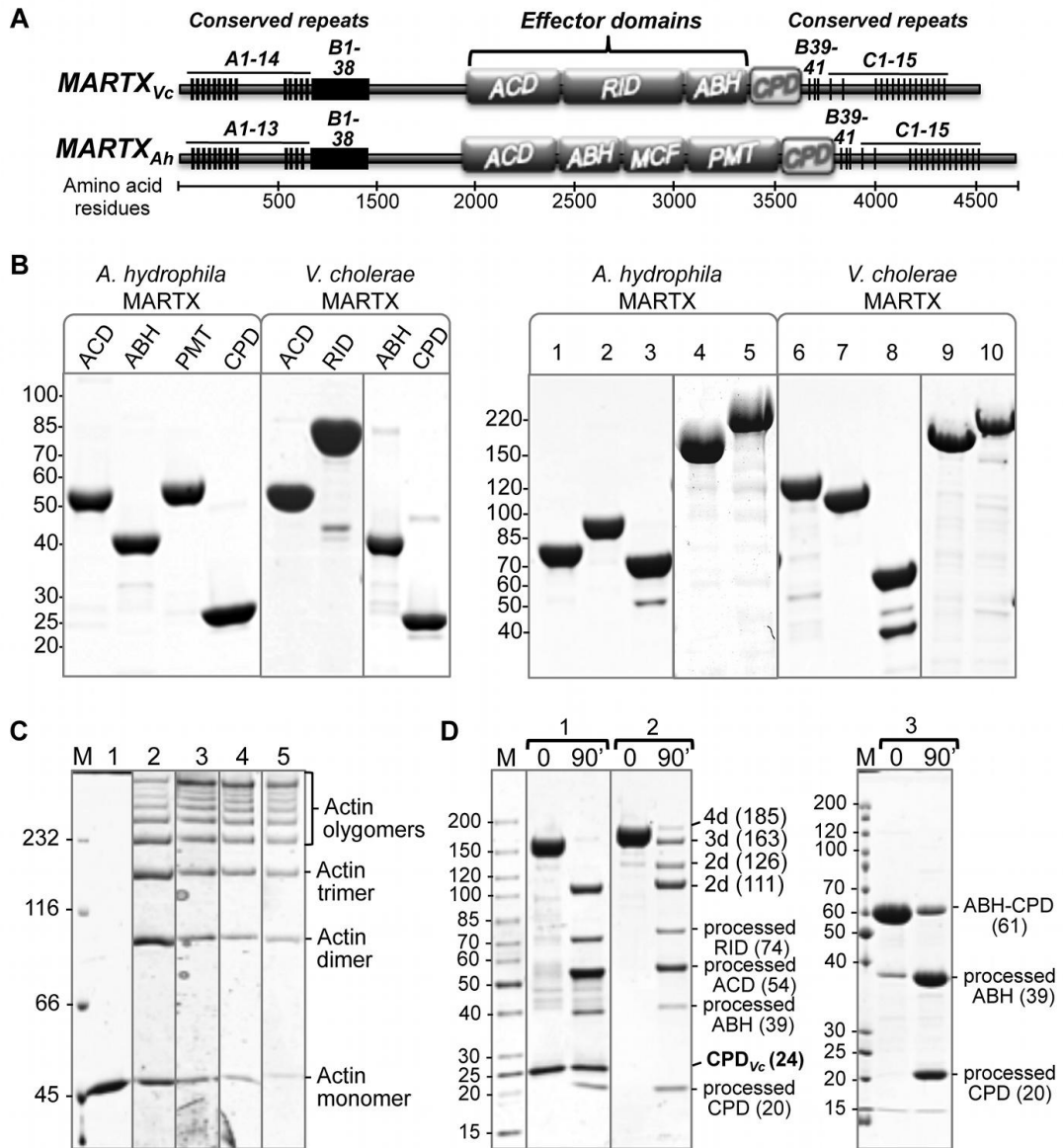
<i>Domains</i>	<i>MW, kDa</i>	<i>Position in the MARTX_{Vc} (AAD21057.1) or MARTX_{Ah} (YP_855898.1)*</i>	<i>Secondary structure T_m (°C) by far UV CD (T aggregation)**</i>	<i>Tertiary structure T_m (°C) by DSF</i>	<i>ΔT_m</i>
ACD _{Vc}	54.0	1959-2434	53.6 (51)	39.7±1.5	14
RID _{Vc}	74.7	2435-3085	45.1 (56)	34.2±1.6	11
ABH _{Vc}	38.8	3086-3428	44.3 (n/a)	36.3±0.4	8
CPD _{Vc}	24.2	3429-3631	53.8 (n/a)	47.7±1.6	6
ACD-RID _{Vc}	126.6	1959-3085	48.4 (48)	36.6±1.5	12
RID-ABH _{Vc}	111.4	2435-3428	43.0 (n/a)	37.7±1.0	5
ABH-CPD _{Vc}	60.9	3086-3631	44.0 (n/a)	36.5±1.4	7.5
ACD-RID-ABH _{Vc}	163.2	1959-3428	43.1 (49)	36.3±0.8	7
ACD-RID-ABH-CPD _{Vc}	185.3	1959-3631	43.4 (n/a)	37.3±0.7	6
ACD _{Ah}	53.0	1925-2391	40.2 (38)	27.4±1.7	13
ABH _{Ah}	40.1	2392-2744	46.3 (45)	44.0±0.6	2
PMT _{Ah}	60.4	3046-3580	43.2 (42)	42.2±2.0	1
CPD _{Ah}	24.5	3581-3786	60.0 (n/a)	51.0±1.4	9
ACD-ABH _{Ah}	80.2	1925-2647	37.3 (35)	25.4±0.6	12
MCF-PMT _{Ah}	105.0	2648-3580	38.0 (36)	34.3±0.6	4
PMT-CPD _{Ah}	82.7	3046-3786	41.5 (39)	38.4±0.9	3
ACD-ABH-MCF-PMT _{Ah}	182.2	1925-3580	39.7 (39)	30.7±0.4	9
ACD-ABH-MCF-PMT-CPD _{Ah}	204.5	1925-3786	37.4 (36)	28.2±0.7	9.2

895

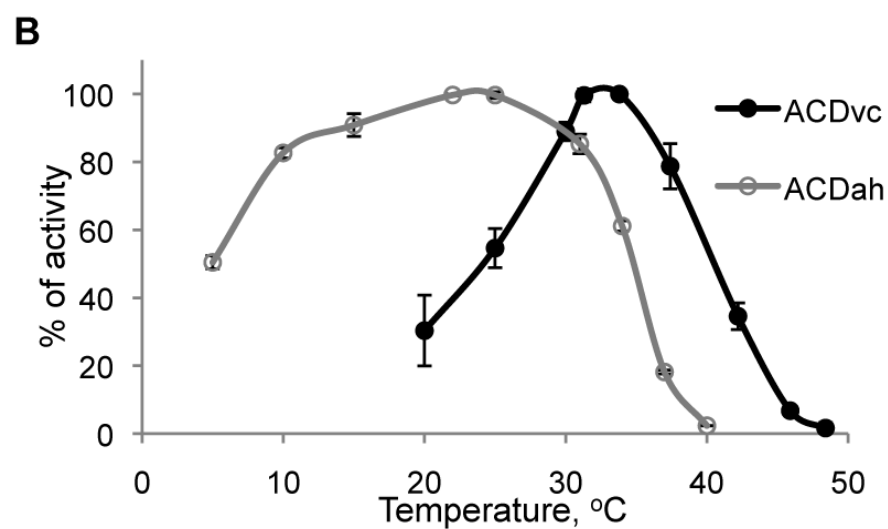
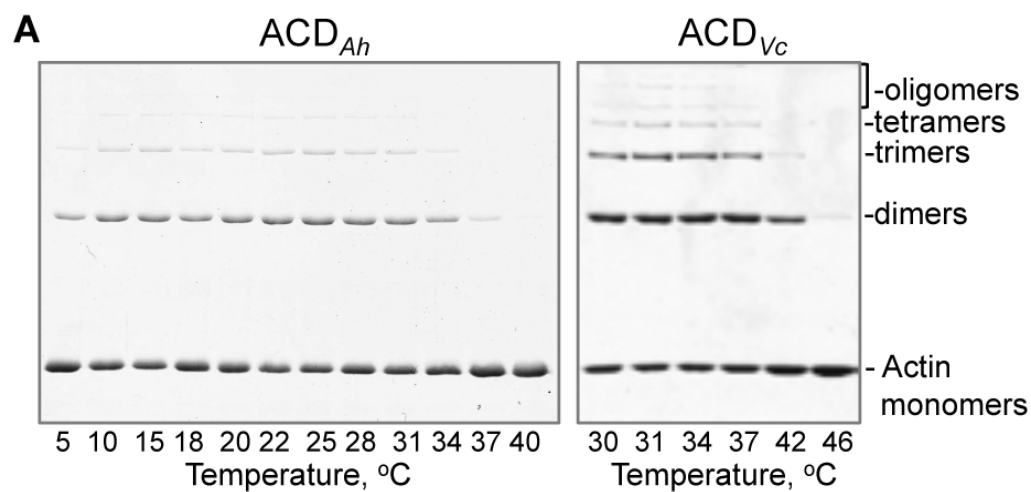
896 * – NCBI accession numbers for protein sequences of MARTX_{Vc} and MARTX_{Ah} toxins are
897 shown in parentheses.898 ** – temperature of protein aggregation as determined by mid-point transition of dynode
899 voltage curve.900 T_m – protein melting temperature as determined by mid-point transition of far-UV CD or DSF
901 fluorescence curves. Aggregation temperatures are given in parenthesis.902 ΔT_m – difference between melting temperatures of secondary and tertiary structures
903 determined by far-UV CD and DSF, respectively.

904 MW – protein molecular weight (including the N-terminal 6xHis tag).

905 n/a – not applicable.



mmi_12615_f1

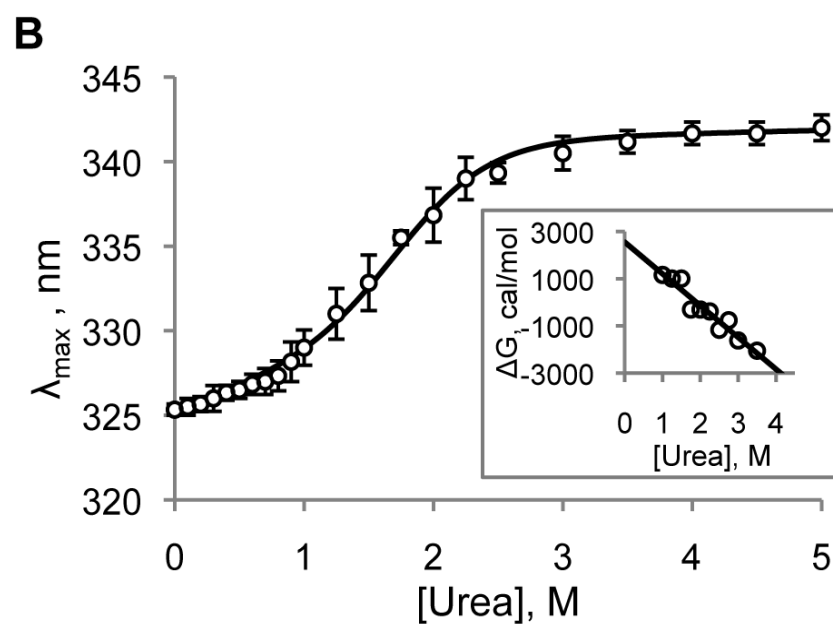
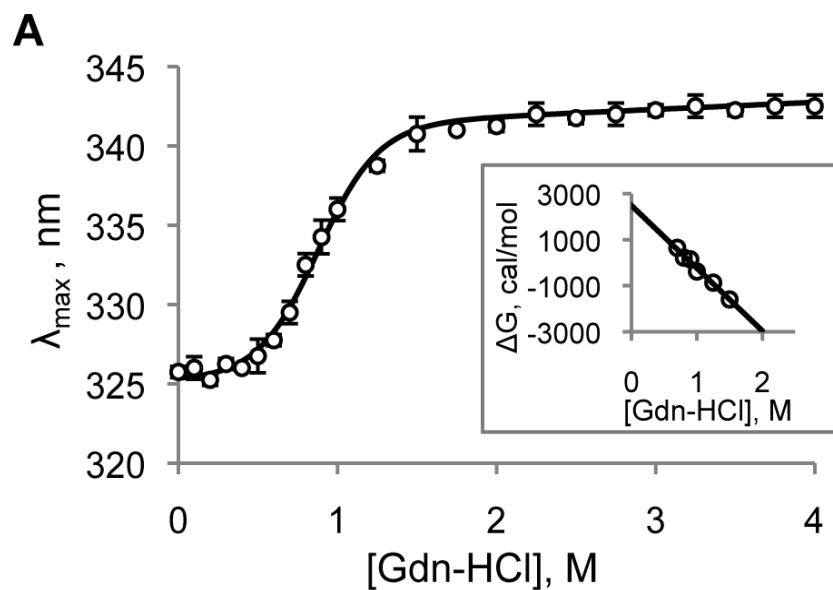


909

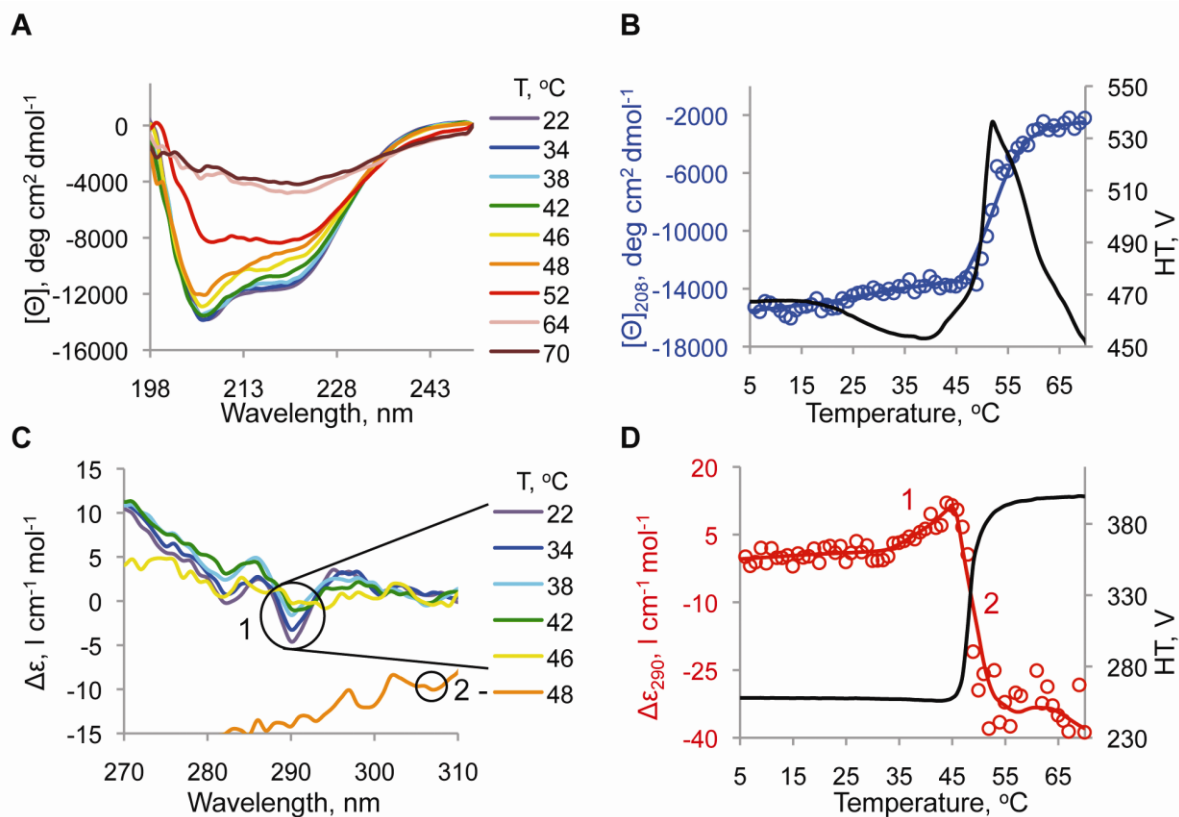
910

911

mmi_12615_f2



mmi_12615_f3

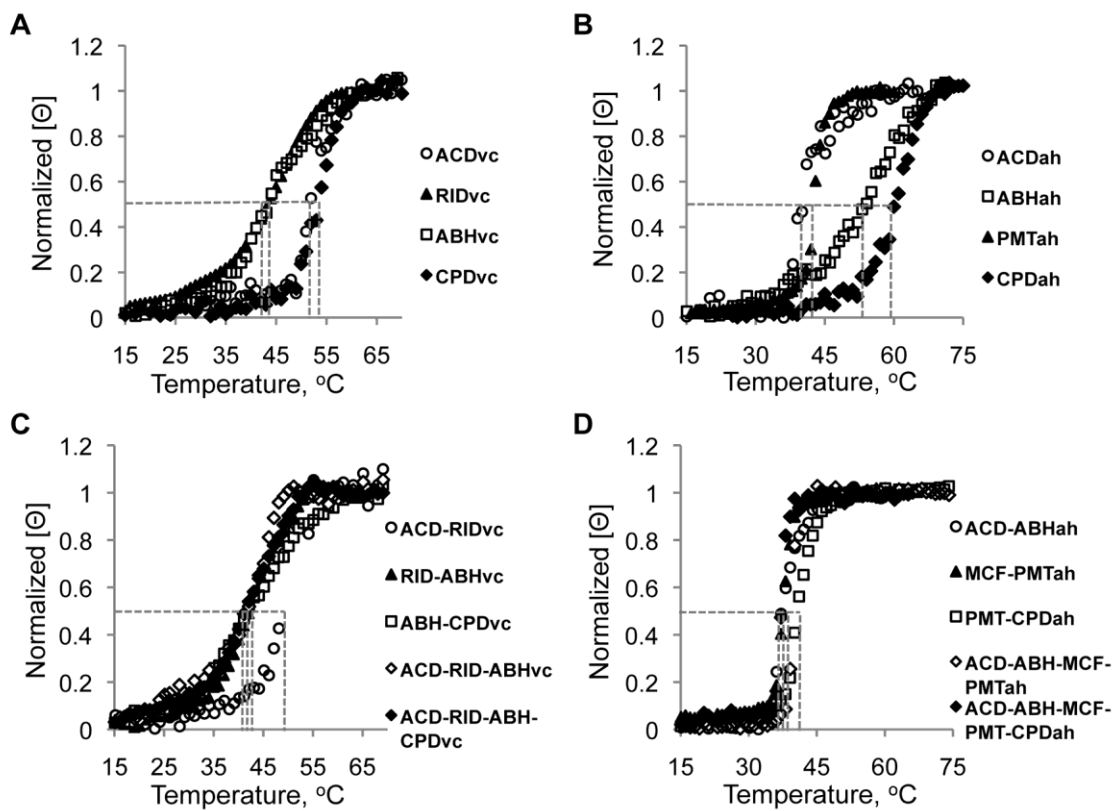


916

917

918

mmi_12615_f4

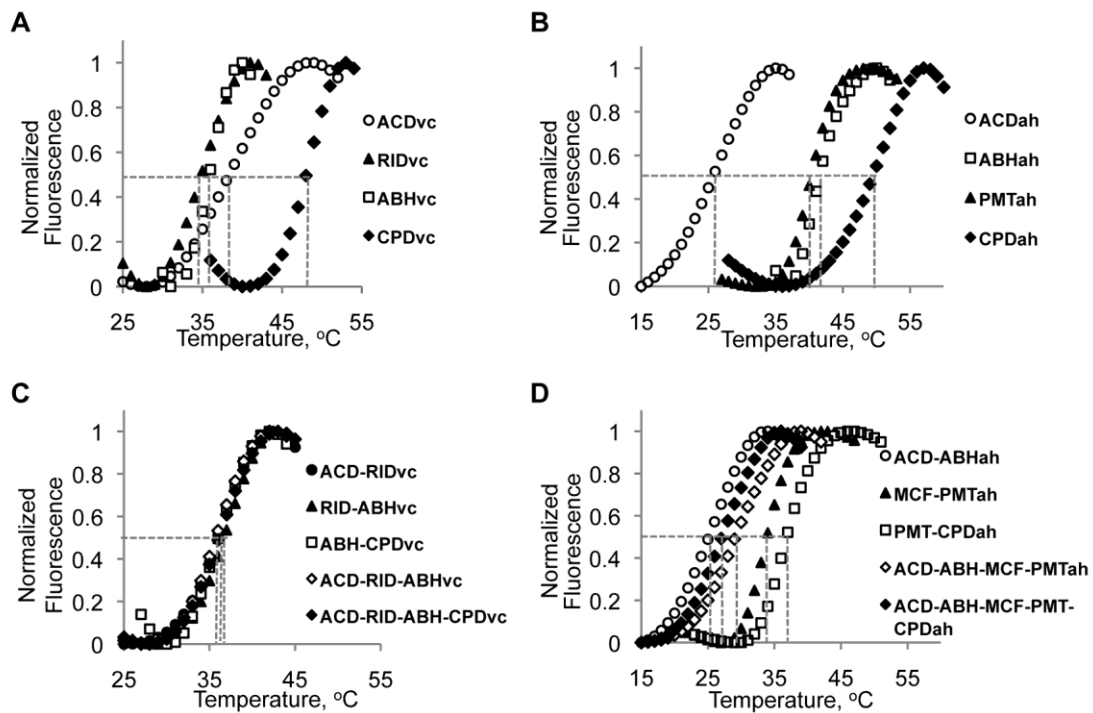


919

920

921

mmi_12615_f5

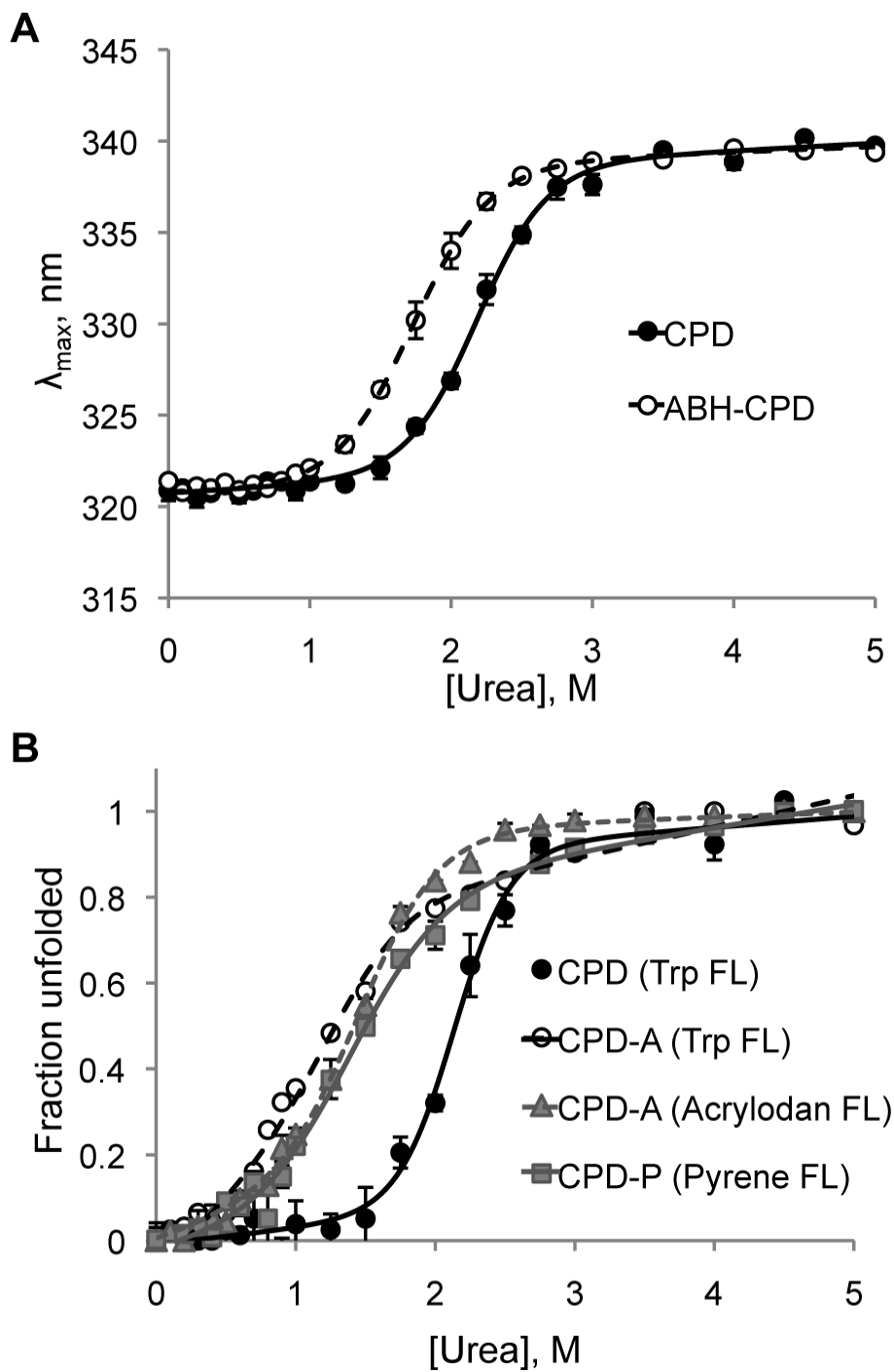


922

923

924

mmi_12615_f6



925

926

927

mml_12615_f7